Geoscience Frontiers 14 (2023) 101623

Contents lists available at ScienceDirect

Geoscience Frontiers

journal homepage: www.elsevier.com/locate/gsf

Research Paper

Tidal drag and westward drift of the lithosphere

Vincenzo Nesi [a,b], Oscar Bruno [c], Davide Zaccagnino [d], Corrado Mascia [a], Carlo Doglioni [b,d,*]

[a] Dipartimento di Matematica Guido Castelnuovo, Piazzale Aldo Moro, 5, Roma 00185, Italy
[b] Istituto Nazionale di Geofisica e Vulcanologia, Via di Vigna Murata, 605, Roma 00143, Italy
[c] Computing and Mathematical Sciences Department, Caltech, 1200 E. California Blvd., MC 305-16, Pasadena 91125, CA, USA
[d] Dipartimento di Scienze della Terra, Piazzale Aldo Moro, 5, Roma 00185, Italy

ARTICLE INFO

Article history:
Received 20 February 2023
Revised 12 April 2023
Accepted 21 April 2023
Available online 27 April 2023
Handling Editor: M. Santosh

Keywords:
Tidal drag
Plate motions
Polarized plate tectonics
Lithosphere-asthenosphere interaction

ABSTRACT

Tidal forces are generally neglected in the discussion about the mechanisms driving plate tectonics despite a worldwide geodynamic asymmetry also observed at subduction and rift zones. The tidal drag could theoretically explain the westerly shift of the lithosphere relative to the underlying mantle. Notwithstanding, viscosity in the asthenosphere is apparently too high to allow mechanical decoupling produced by tidal forces. Here, we propose a model for global scale geodynamics accompanied by numerical simulations of the tidal interaction of the Earth with the Moon and the Sun. We provide for the first time a theoretical proof that the tidal drag can produce a westerly motion of the lithosphere, also compatible with the slowing of the Earth's rotational spin. Our results suggest a westerly rotation of the lithosphere with a lower bound of $\omega \approx (0.1 - 0.2)^{\circ}$/Myr in the presence of a basal effective shear viscosity $\eta \approx 10^{16}$ Pa·s, but it may rise to $\omega > 1^{\circ}$/Myr with a viscosity of $\eta \lesssim 3 \times 10^{14}$ Pa·s within the Low-Velocity Zone (LVZ) atop the asthenosphere. This faster velocity would be more compatible with the mainstream of plate motion and the global asymmetry at plate boundaries. Based on these computations, we suggest that the super-adiabatic asthenosphere, being vigorously convecting, may further reduce the viscous coupling within the LVZ. Therefore, the combination of solid Earth tides, ultra-low viscosity LVZ and asthenospheric polarized small-scale convection may mechanically satisfy the large-scale decoupling of the lithosphere relative to the underlying mantle. Relative plate motions are explained because of lateral viscosity heterogeneities at the base of the lithosphere, which determine variable lithosphere-asthenosphere decoupling and plate interactions, hence plate tectonics.

© 2023 China University of Geosciences (Beijing) and Peking University. Published by Elsevier B.V. on behalf of China University of Geosciences (Beijing). This is an open access article under the CC BY-NC-ND license (http://creativecommons.org/licenses/by-nc-nd/4.0/).

1. Introduction

The mechanisms controlling plate tectonics are still controversial, ranging from bottom-up to top-down mantle convection (e.g., Anderson, 2001, and references therein). The current technique to measure the motion of the lithosphere is based on the Global Navigation Satellite System (GNSS), having the theoretical assumption that the sum of the kinematics of all plates equals zero, i.e., the no-net-rotation (NNR) reference frame (Teunissen and Montenbruck, 2017; Weiss et al., 2017). This mathematical requirement provides very accurate data on the relative movements among plates. However, the motion of the lithosphere relative to the mantle remains unsolved. In fact, the hotspot reference frame (HSRF) rather shows that the sum of all plate velocities is not null, recording a westerly directed residual, which is inferred to be small ($0.1^{\circ} - 0.4^{\circ}$/Myr) in the deep HSRF, and much faster ($1.0^{\circ} - 1.5^{\circ}$/Myr) in the shallow intra-asthenospheric HSRF (Doglioni et al., 2005; Cuffaro and Doglioni, 2007; Crespi et al., 2007). Regardless the origin and source depth of the hotspots, e.g., the shallow wetspots (Bonatti, 1990), the westward drift origin remains physically unexplained, although GNSS baselines suggest a solid Earth tidal modulation of plate motions; in fact, tidal harmonics seem to modulate plate motions and their speed (Zaccagnino et al., 2020). Moreover, plate boundaries show a geographically tuned asymmetry that is consistent with the westerly drift of the whole lithosphere relative to the underlying mantle, and the mainstream of plate motions supports a shallow source of the hotspots (Doglioni, 1993; Doglioni and Panza, 2015). The westward drift of the lithosphere was postulated by Le Pichon (1968) and invoked as the effect of the tidal drag (Bostrom, 1971; Nelson and Temple, 1972), being responsible for the asymmetry of the Pacific slabs (Uyeda and Kanamori, 1979; Doglioni, 1992; Riguzzi et al., 2010; Ficini et al., 2017), whereas Doglioni

* Corresponding author.
E-mail address: carlo.doglioni@uniroma1.it (C. Doglioni).

https://doi.org/10.1016/j.gsf.2023.101623
1674-9871/© 2023 China University of Geosciences (Beijing) and Peking University. Published by Elsevier B.V. on behalf of China University of Geosciences (Beijing). This is an open access article under the CC BY-NC-ND license (http://creativecommons.org/licenses/by-nc-nd/4.0/).

(Doglioni, 1990) suggested the existence of a mainstream along which plates move, having a primary rotation and sub-rotations (Cuffaro et al., 2008). Plate tectonics is controlled by the influence of lateral variations of viscosity at the interface between lithosphere, asthenosphere and upper mantle itself. These gradients allow variable amounts of relative motion between Earth's layers, hence, plate velocity. If there were a perfectly uniform global mechanical coupling between lithosphere and mantle, then, ideally, the lithosphere would behave as a single shell with no internal relative velocities, so, there would be no surface plate interaction, i.e., plate tectonics. Based on the velocities of the GNSS stations and the hinge behavior of the subduction zones, nowadays it is possible to calculate the volumes of lithosphere wedged into the Earth's mantle: they are about 300±30 km^3/yr (Doglioni and Anderson, 2015; Ficini et al., 2020). Even in this case, there is an asymmetry. In fact, the volumes subducting towards the west are more than 214±21 km^3/yr; the difference is for the easterly-oriented subductions that provide about three times smaller mantle volume contribution. Therefore, a difference in recycling between the two systems implies an unbalance of mass which should be compensated, so the Earth's mantle must relatively migrate from west to east to fill the mass unbalance. Asymmetries also affect geometries, dynamics of geological structures and seismic activity. Subduction zones are paradigmatic by this viewpoint: they are steeper if westerly directed (mean angle of dip about $65° \pm 4°$) than those with opposite polarity ($27° \pm 3°$; Riguzzi et al., 2010). Moreover, westerly oriented subduction zones are associated with back-arc spreading, passive margins, and volcanic arcs with low topography; conversely, east-directed subductions have trenches located besides large orogens (Lenci and Doglioni, 2007). The orogens associated with easterly-directed subduction zones are about 5–10 times larger than the accretionary prisms related to westerly-directed subduction zones. This implies that the decollements are deeper and exhume larger volumes along easterly-oriented subduction zones than those with opposite polarity. Not only subductions and accretionary prisms: asymmetries affect back-arc basins with concave geometry at the western margin opposed to the convexity of the external arc. Despite this multifaceted evidence, the astronomical contribution to plate tectonics remains unsolved and mostly neglected, even though the role of tidal perturbations has been highlighted to play a role in crustal stability, e.g., Kossobokov and Panza (2020), because the inferred viscosity of the asthenosphere would be too high to allow the tidal drag to be efficient (e.g., Jordan, 1974). Nevertheless, the lithosphere is significantly decoupled from the underlying mantle, being able to move relatively to it up to several centimeters per year. One of the most straightforward proofs of this phenomenon is that the fastest-moving plates are those showing lower basal viscosity (e.g., the Pacific plate has about 10^{17} Pa s (Pollitz et al., 1998; Becker, 2017)). The long-term trend of motion of the lithosphere appears to be oriented along a main flow described by the so-called 'tectonic equator', which is approximately a circle forming an angle of about 30° with the geographic equator (Crespi et al., 2007). A possible explanation may be provided by the Maxwell time of the lithosphere that behaves like a fluid sensitive to the timeframe of the precession of the Earth axis, and the low viscosity within the low velocity zone (LVZ) constraining the mechanical decoupling between the lithosphere and the underlying mantle (Doglioni and Panza, 2015). That is, lateral rheological heterogeneities in the plane of uncoupling control the velocity gradients between plates and thus seismicity. All these observations are consistent with a polarized plate tectonics, i.e., with the lithosphere moving relatively westward relative to the underlying mantle. However, no one of the forces usually advocated as drivers of global plate tectonics can produce the worldwide asymmetric pattern (Zaccagnino and Doglioni, 2022). This suggests that the effect of an additional force may be crucial for solving the puzzle of absolute plate motions. In this article, we provide a new mathematical computation of the lunar and solar tidal drag; moreover, we select the most likely values of the parameters which play a key role in large scale geodynamics and compatible with observations. In view of this astronomical frame, we then provide a conceptual model of the asthenosphere and its upper layer, the low-velocity zone (LVZ), combining the external and internal phenomena, which appear generating a strongly interacting self-organized chaotic system governing plate tectonics (Doglioni et al., 2007; Riguzzi et al., 2010).

2. Tidal drag modeling

The tidal acceleration on a point of the Earth, p, due to the gravitational effect of the Moon from e is given by

$$a_{\mathrm{m}}(p,e) = r_{1,p}\,\Omega_{\mathrm{m}}^2\,[3\cos(\varphi - \beta_{\mathrm{m}}(t))\,\hat{u}(\beta_{\mathrm{m}}(t)) - \hat{u}(\varphi)] \tag{1}$$

where $\Omega_{\mathrm{m}}^2 = \frac{Gm_{\mathrm{m}}}{(d_{\mathrm{e,m}})^3}$, m_{m} represents the mass of the Moon, $r_{1,p}$ stands for the position of the observation point p in the reference frame of the Earth (see Appendix B), $d_{\mathrm{e,m}}$ is the distance of the Moon from the center of Earth and G stands for the universal gravitational constant. We use the angular variable φ in order to describe the relative position of the Moon with respect to the Earth in the inertial system, while $\beta_{\mathrm{m}}(t)$ is a temporal parameter. For a detailed description of the meaning of different symbols, see Appendix A and B. Such an acceleration is responsible for a force deforming the Earth as a function of the Moon position and complex interactions between the celestial body and the solid and fluid components of our planet. Nonetheless, the shape of the Earth is in a quasi-equilibrium configuration, being just weakly perturbed by the tidal potential. While great part of the deformation acts elastically, so that the mechanical response of the system is almost instantaneous, a part of it shows a viscous behavior (compare with the session "Discussion") producing an angular delay usually estimated in the order of a few degrees ($0.2° - 2°$). Hence, in order to model the effect of the tidal potential on our planet and to understand its geodynamic implications, we need to introduce a viscoelastic force that opposes the rotational motion of the Earth. To describe its analytical form, we consider the average angular delay using the so-called tidal lag, henceforth ε. Therefore, we assume that, with respect the unperturbed Earth's surface, at a certain instant, the tidal deformation has the shape of a sine wave $h(t)$ with a very large wavelength. The two highest peaks move on the Earth's surface according to the equation

$$\max_t h(t) = h(\beta_{\mathrm{m}} + \varepsilon) = h(\beta_{\mathrm{m}} + \pi + \varepsilon) \tag{2}$$

$t \to \beta_{\mathrm{m}}(t)$ parameterizes the position of the Moon. The tidal brake produces a damping factor of the tangential acceleration whose maximum is located where the function h is minimum, i.e., at the points where the physical Earth bulge is at its minimum elongation. We also observe that the normal component of the tidal brake is irrelevant since it acts symmetrically in its up and down components. In Fig. 1, we show the tidal vector field due to the Moon (not to scale) and its tangential component with (Fig. 1b) or without (Fig. 1d) the effect of the tidal brake. These considerations lead to conjecture that the tangential component of the tidal brake acceleration has the form (See Fig. 1d)

$$a_{\mathrm{tang}} = -r_{1,p}\,\omega_{\mathrm{lag}}^2\cos(\varphi - \beta_{\mathrm{m}} + \varepsilon) \tag{3}$$

where, for physical reasons,

$$\omega_{\mathrm{lag}}^2 = 3\,\delta\,\Omega_{\mathrm{m}}^2, \quad \delta \in (0,\ 1) \tag{4}$$

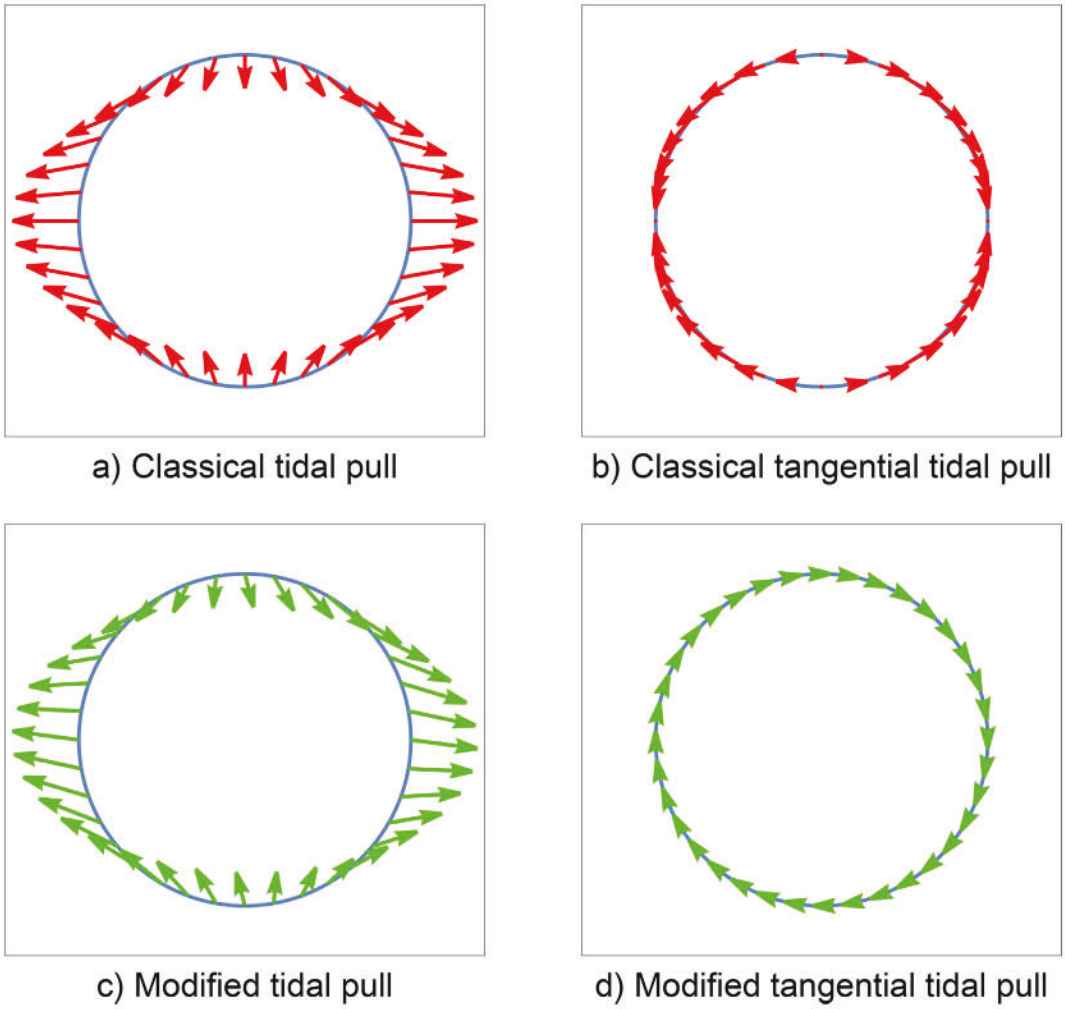

Fig. 1. Tidal potential and its tangential component in the case of perfectly elastic response of the Earth to tides (a,b) and in the case of a viscous component (c,d).

Fig. 2 illustrates the physical meaning of the decoupling parameter, henceforth δ. The blue curve represents the damping effect due to the vertical load produced by the normal component of the gravitational force. If such a component points inward with respect to the surface of the Earth, the motion becomes slower. We are now ready to write the equation for our model including the effect of a mechanical decoupling between the inner and outer layers due to rheological weakness in the asthenosphere (compare with the introduction and discussions for the geological meaning and physical motivation). We introduce the subscript δ_{m} to indicate we are treating the case in which only the Moon is considered. Later we will include Sun and Moon simultaneously. We have

$$a_{\mathrm{m}}(p,e,\varepsilon_{\mathrm{m}},\delta_{\mathrm{m}}) := a_{\mathrm{m}}(p,e) + a(p,e,\varepsilon_{\mathrm{m}},\delta_{\mathrm{m}}) \tag{5}$$

and the tangential acceleration is

$$\begin{aligned} a_{\mathrm{tang}}(p,e) = {} & 3 r_{1,p} \Omega_{\mathrm{m}}^2 \sin(\beta_{\mathrm{m}} - \varphi_{1,p})[\cos(\varphi_{1,p} - \beta_{\mathrm{m}}) \\ & - \delta_{\mathrm{m}} \cos(\varphi_{1,p} - \beta_{\mathrm{m}} + \varepsilon_{\mathrm{m}})] \end{aligned} \tag{6}$$

The changes that result from taking into account the moment produced by the tidal torque lead to the following formula:

$$\begin{aligned} & \ddot{\Phi} + 3\,\Omega_{\mathrm{m}}^2 \sin(\Phi - \gamma_{\mathrm{m}} t + \beta_{\mathrm{m}})[\cos(\Phi - \gamma_{\mathrm{m}} t + \beta_{\mathrm{m}}) \\ & - \delta_{\mathrm{m}} \cos(\Phi - \gamma_{\mathrm{m}} t + \beta_{\mathrm{m}} - \varepsilon_{\mathrm{m}})] = 0 \end{aligned} \tag{7}$$

where $\Phi = -\varphi + \gamma_{\mathrm{m}} t$, $\gamma_{\mathrm{m}} = \frac{2\pi}{T_{\mathrm{D}}} - \frac{2\pi}{T_{\mathrm{M}}}$ with T_{D} the period of the diurnal tidal harmonics and T_{M} the period of the monthly lunar harmonics. The variable is measured in the reference system in which the Earth is at rest (see Appendix B). The convention is that the westward direction corresponds to increasing Φ. We also assume that at the initial configuration its position is represented by $\varphi = 0$. See Appendix A for the meaning of parameters. The last ingredient needed to complete the mathematical framework is a viscous term due to friction acting between contiguous layers inside the Earth. Here, we assume a linear frictional term as a first hypothesis, even though such choice is likely to be too severe. In addition, we eventually consider the simultaneous effect of Moon and Sun, so that our model equation eventually reads

$$\begin{cases} \Phi_{tt} + K\Phi_t + \\ +3 \sum\limits_{i=\mathrm{m,s}} \Omega_i^2 \sin(\Phi - \gamma_i t - \beta_i(0))[\cos(\Phi - \gamma_i t - \beta_i(0)) \\ \qquad -\delta_i \cos(\Phi - \gamma_i t - \beta_i(0) - \varepsilon_i)] = 0 \\ \Phi(0) = q, \quad \Phi_t(0) = 0 \end{cases} \tag{8}$$

where $\Omega_i^2 = \frac{Gm_i}{(d_{e,i})^3}$, m_i represents the mass of the Moon ($i = \mathrm{m}$) or the Sun ($i = \mathrm{s}$), $d_{e,i}$ is the distance of the celestial body from the center of Earth (see Appendix A). The apparent motions of the Moon and the Sun around the Earth are described by $t \to \beta_{\mathrm{m}}(t)$ and $t \to \beta_{\mathrm{s}}(t)$ respectively. $\Omega_{\mathrm{m}}^2, \Omega_{\mathrm{s}}^2$ depend on the gravitational constant G and on the masses of the Moon and Sun respectively.

Now, we are interested in the motion of plates, i.e., large portions of the surface of the Earth. We can represent them, as a first approximation, as arcs of circumference, say γ, of semi-opening $\alpha \in (0, \frac{\pi}{2})$. The center of mass of γ moves on a smaller circumference, i.e., at a fixed distance from the center of the Earth. Therefore, the motion is completely determined by just one angle that we choose to be the average one, φ_c, so that γ is described by $\varphi \in (\varphi_c - \alpha, \varphi_c + \alpha)$. Then, assuming the plate be almost rigid, the first cardinal equation implies that the law $t \to \Phi_c(t)$ relative to the center of mass of the arc γ can be considered representative of the motion of the whole plate. Using some trigonometric identities and introducing the new definitions

$$Y(t) = \Phi(t) - \Phi(0) - \omega_{m,s}\, t,$$
$$\omega_{m,s} = \frac{3\Omega_m^2\, \delta_m\, \sin\varepsilon_m + 3\Omega_s^2\, \delta_s\, \sin\varepsilon_s}{2K} \tag{9}$$

we get that Eq. (8) is equivalent to

$$\begin{cases} Y_{tt} + KY_t + + \sum\limits_{i=m,s} \frac{3\Omega_i^2(1-\delta_i\cos\varepsilon_i)}{2} \sin\left[2\left(Y - l_i(t)\right)\right] \\ \qquad + \sum\limits_{i=m,s} \frac{3\Omega_i^2\,\delta_i\,\sin\varepsilon_i}{2} \cos\left[2\left(Y - l_i(t)\right)\right] = 0 \\ Y(0) = 0, \quad Y_t(0) = 0 \end{cases} \tag{10}$$

with

$$l_i(t) = \beta_i(0) - q + (\gamma_i - \omega_i)\, t \tag{11}$$

By construction, the solution Φ to Eq. (8) reads

$$\Phi(t) - \Phi(0) = \omega_{m,s}\, t + Y(t) \equiv L(t) + Y(t) \tag{12}$$

The physical meaning of Y represents the detrended modulation of the cumulative tidal displacement of plates with respect to the deep mantle, Φ, around the linear trend $L(t)$ defined just above. At last, let us give the Eq. (10) a slightly more compact, but explicit expression by introducing new variables (see Appendix A for details) and using some additional transformations:

$$\begin{cases} Y_{tt} + KY_t + (c_m^2 + d_m^2)\, \sin\left[2\left(Y - L_m(t)\right)\right] \\ \qquad + (c_s^2 + d_s^2)\, \sin\left[2\left(Y - L_s(t)\right)\right] = 0 \\ Y(0) = 0, \quad Y_t(0) = 0 \end{cases} \tag{13}$$

Since the tidal lag is only a function of the mechanical properties of Earth without any effect due to the action of other celestial bodies, $\delta_s = \delta_m = \delta$ (also compare with the discussion section for a more detailed physical justification) and $\varepsilon_s = \varepsilon_m = \varepsilon$.

3. Results

3.1. Tidal modulations of plate motions as a function of viscosity and harmonic period

We now present the numerical simulations for the oscillating component of Φ, i.e., the solution Y of Eq. (13) and Φ itself in detail. Concerning the residual displacement, we plot the diurnal, monthly and annual solution assuming $K = 100\ \mathrm{s}^{-1}$(corresponding to $\eta \approx 5 \times 10^{15}$ Pa·s), and $\varepsilon = 1°$. Our results reported in Fig. 3 clearly show that high frequency tides are not able to provoke any detectable effect on plate motions with respect to the deep mantle, as expected. Of course, tides produce elastic displacement up to several decimeters, but they do not affect absolute plate velocity. Numerically, we also observe that the detrended solution Y is bounded by a constant B_{max} that depends on the frictional parameter K (which is related to the basal viscosity of the lithosphere - compare with paragraph 3.2) but also on δ_s and δ_m. The bigger (i.e., the closer to one) δ_s and δ_m are, the smaller B_{max}. Conversely, the smaller K (i.e., the closer to zero), the bigger B_{max}. By a physical point of view, large values of δ's make the oscillatory force smaller and smaller. Conversely, higher friction should enhance stronger damping. The bound B_{max} has a physical meaning: it provides an estimation of the amplitude of tidal displacement acting while the motion proceeds westward. Thus, we want to have B_{max} of the order of the observed fluctuations, i.e., compatible with noise for high frequency tides. The regime we want to study is in the range $K \in [1, 100]$. Of course, the smaller K, the faster the plates move. On the other hand, the bigger the friction K is the smaller the high-frequency modulations are. For $K \in [1, 100]$ the maximum oscillation is of the order of that occurring in one day. Therefore, we propose the theoretical bound

$$B_{max} \leq \frac{\varepsilon_m + \varepsilon_s}{K} \tag{14}$$

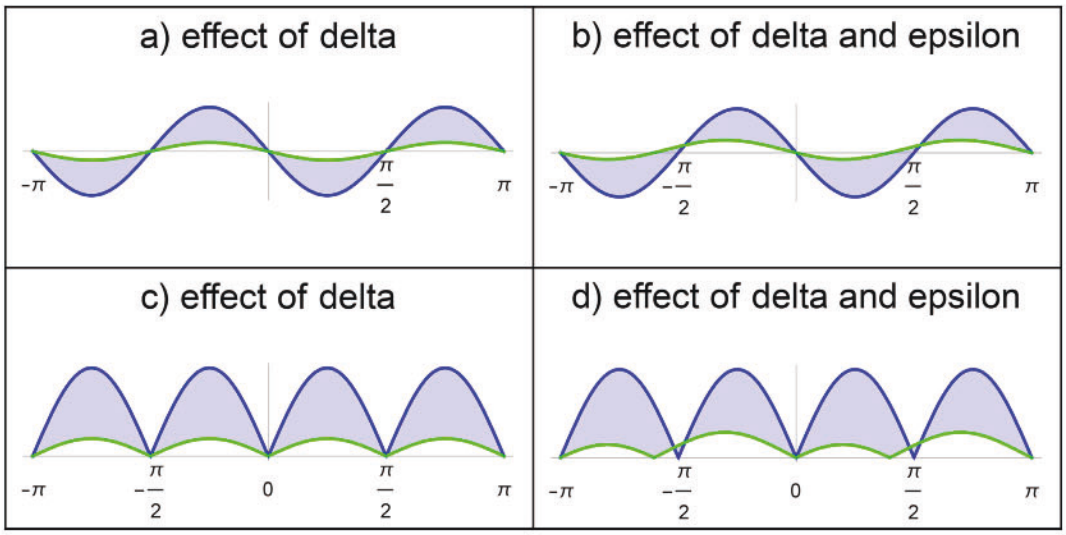

Fig. 2. Illustration not to scale, for better visualization, of the physical meaning of the decoupling parameter δ. (a) The green curve represents the damping effect with respect to the acting perturbation (blue line) due to the vertical load produced by the normal component of the gravitational force. If such a component points inward with respect to the surface of the Earth, the motion becomes slower. (b) This panel shows the break of symmetry of the potential field obtained using the difference of the angle formed by the actual Earth high tide with the position of the Moon at its Zenith (tidal lag). (c,d) Taking the absolute value of the perturbation makes more evident both the angle shift ε and the asymmetry around the equilibrium position.

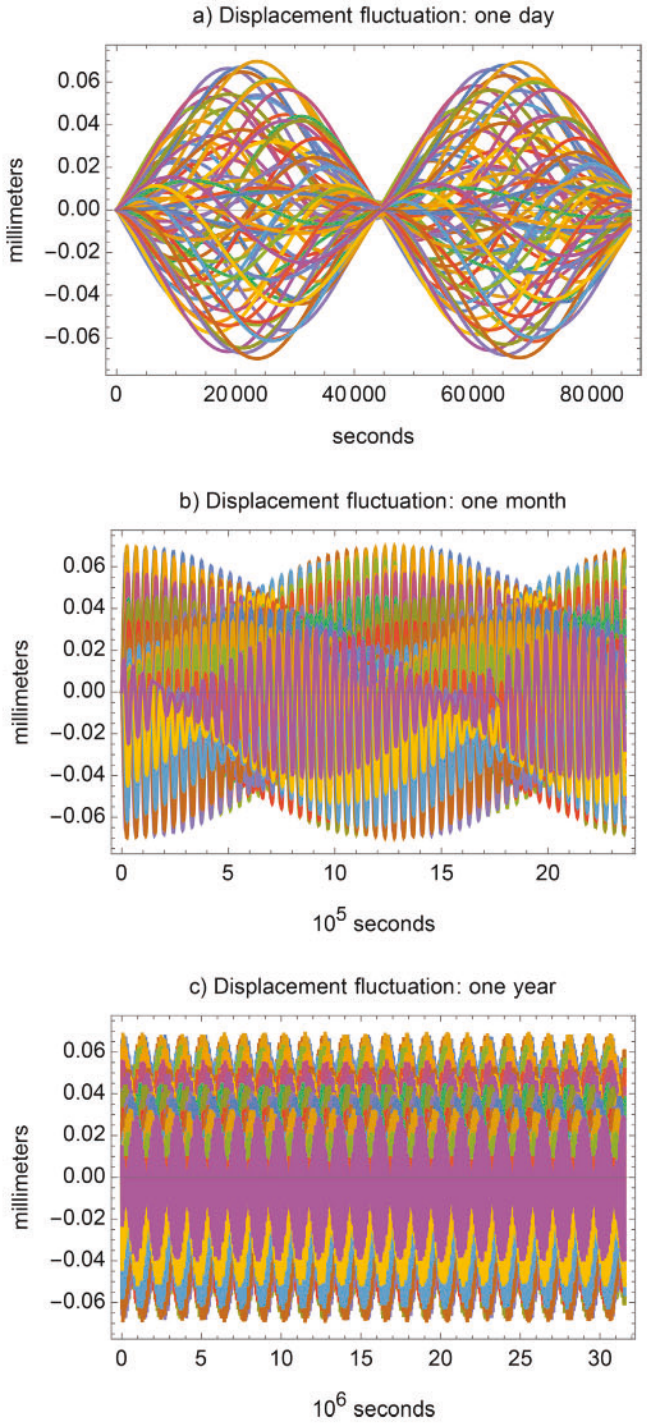

Fig. 3. Solutions of the residual of Solid Earth tidal displacements calculated assuming $K = 100\ s^{-1}$ ($\eta = 5 \times 10^{15}$ Pa·s), $\delta_s = \delta_m = 1$ for intervals of one day (a), one month (b) and one year (c).

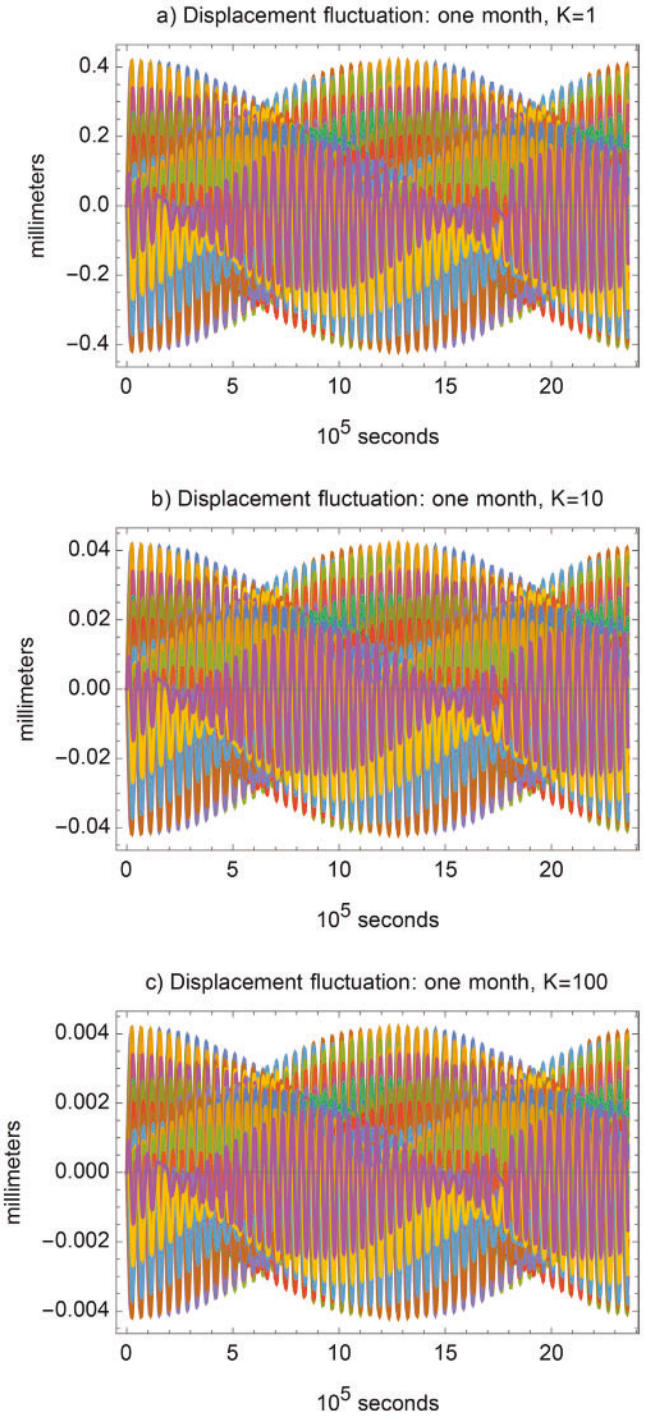

Fig. 4. Residual displacement around the linear trend for increasing values of K compared with $\pm \frac{\delta_m + \delta_s}{K}$. We choose $K = 1, 10, 100\ s^{-1}$, corresponding to an effective shear viscosity of about $\eta = 5 \times 10^{13}$, 5×10^{14}, 5×10^{15} Pa·s.

Choosing $K = 100$, $\delta_s = \delta_m \cong 1$ guarantees an angular velocity of about 10^{-16} rad s^{-1} with a basal diurnal fluctuation of about 10^{-3} mm, i.e., completely negligible with respect to the usual sources of deformation produced by other external agents such as hydrological and thermal loading. Compare with Fig. 4. Now, we consider the solution, $\Phi(t)$ of Eq. (8) and make a plot of $\Phi(t) - \Phi(0)$ computing it as the sum of the linear part $L_\infty(t) = \omega_{m,s}\, t$, see Eq. (12), and the bounded component $Y(t)$, solution of Eq. (13) for different time intervals. Using, for instance $K = 25\ s^{-1}$ ($\eta \approx 1.3 \times 10^{15}$ Pa·s), we get a westward motion of about 5 cm/yr.

3.2. On the relationship between K and η

In our model, we introduce the convenient frictional term K; however, the relevant quantity for geodynamics is the effective shear viscosity of the low velocity zone (lower values of viscosity in the asthenosphere), which determines the degree of mechanical coupling between the lithosphere and the underlying layers. Even though it is not possible to provide a exact conversion rule from K to η and viceversa, we are interested in writing a rough correspondence between couples of values. Assuming K to be the frictional

coefficient produced by a viscous force acting on the lithosphere with surface Σ whose mass is represented by m (Fig. 5)

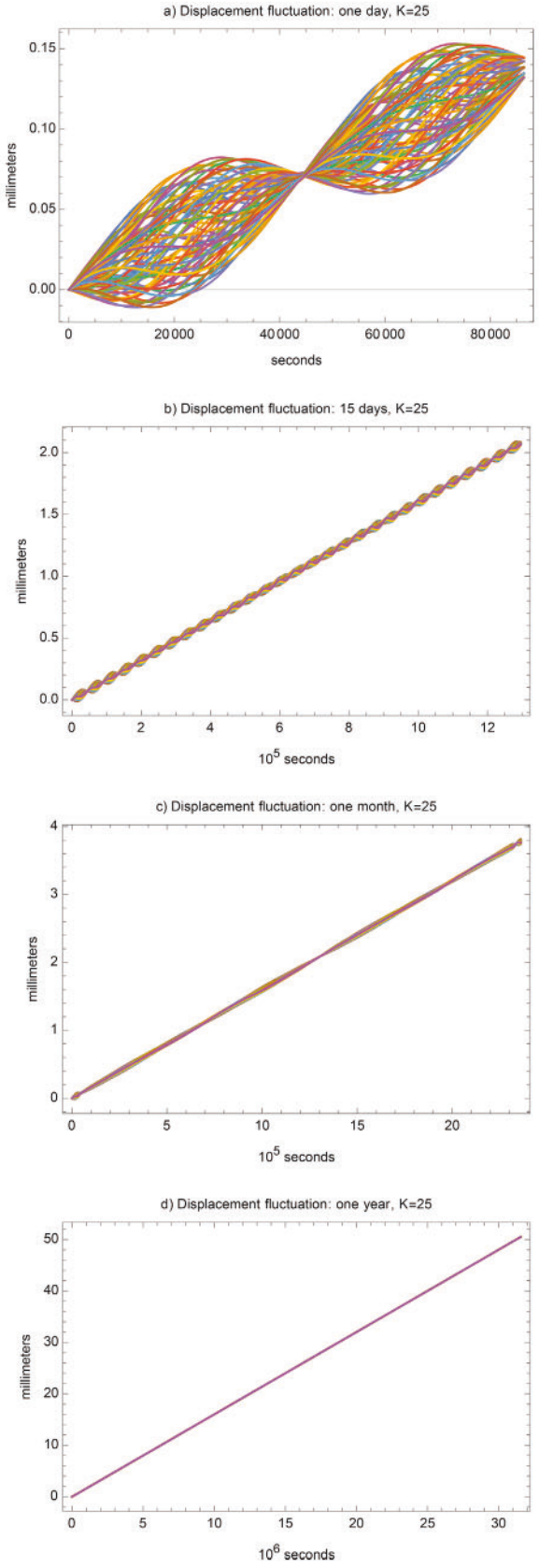

Fig. 5. Expected cumulative displacements produced by the action of the tidal drag assuming $K = 25\ s^{-1}$ ($\eta \approx 1.3 \times 10^{15}$ Pa·s), $\delta_s = \delta_m = 1$ for intervals of one day (a), 15 days (b), one month (c) and one year (d).

$$K = \frac{\Sigma}{D_a m}\eta \tag{15}$$

where $D_a \approx 150$ km is the thickness of the upper asthenosphere. If one takes the lithospheric density $\rho = 3.3$ g/cm^3, η can be written as

$$\eta = D_l D_a \rho K \approx 5 \times 10^{13}\ \text{K Pa} \cdot \text{s} \tag{16}$$

$D_l = 100$ km is the average thickness of the lithosphere. We propose the following theoretical relationship

$$K\omega = \frac{3(\Omega_m^2 + \Omega_s^2)}{2}\sin\varepsilon = \left(1.9 \times 10^{-13}\sin\varepsilon\right)\text{s}^{-2} \tag{17}$$

By physical considerations, we also have:

$$K \cong (2 \times 10^{-14}\eta)\ \text{s}^{-1} \tag{18}$$

Hence,

$$\eta\omega = \left(\frac{1.9}{2.0}\right) * \sin\varepsilon\,\frac{10^{14}}{10^{13}} = 9.5\sin\varepsilon \tag{19}$$

Set

$$\omega = \lambda * 5.5 \times 10^{-16}\,rad\,s^{-1}, \quad \varepsilon_0 = \frac{2\pi}{360}, \quad \varepsilon = t_g\,\varepsilon_0 \tag{20}$$

which gives a relationship for η and ε (Fig. 6), where λ represents the westward drift velocity expressed in °/Myr.

3.3. Low frequency tidal modulations of plate motions

High frequency tidal harmonics are not able to produce a detachment between the lithosphere and the upper mantle since their period is much shorter than the Maxwell's time of the asthenosphere ($\approx 10^9$ s). Therefore, high-frequency body tides are mostly buffered by the high viscosity of the lithosphere and the underlying mantle. Conversely, long-period tides, e.g., the lunar nodal 18.6-years-long precession, can act effectively in modulating plate motions. Our simulations confirm this possibility (Fig. 7), also providing a computational check for the analysis reported in Zaccagnino et al. (2020). The nominal and observed value of

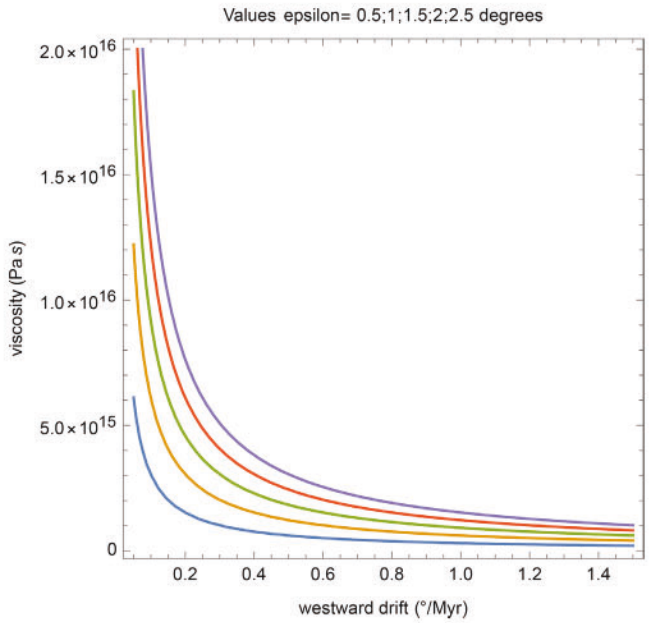

Fig. 6. Westward drift velocity predicted by our model as a function of the basal effective shear viscosity for different tidal lag angles compatible with observations.

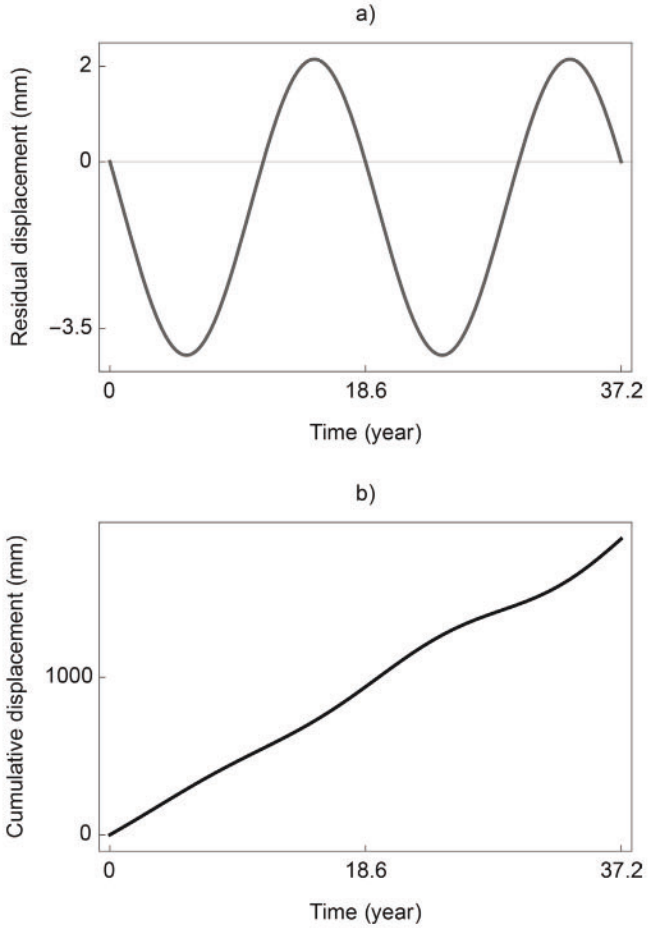

Fig. 7. Tidal modulations of plate motions around the linear long-term trend for $K = 50 s^{-1}$ (corresponding to $\eta \approx 2.5 \times 10^{15}$ Pa·s) produced by the 18.6-years-long tidal harmonic. We notice an almost unfiltered signal (the nominal amplitude of the lunar perigee is about 3 mm) with respect to the strongly buffered perturbations produced by the daily, monthly and annual tides. This suggests that slow additional stress, even though quite small, can act effectively in decoupling the lithosphere from the upper mantle because its period is comparable with the Maxwell's time of the weakest layers of the low velocity zone (LVZ) being of the order of about 10^9 s.

amplitudes, about 3 mm (Agnew, 2010), are correctly reproduced using a viscous frictional term $K \approx 50\ s^{-1}$, corresponding to an effective minimal basal shear viscosity of about $\eta \approx 2.5 \times 10^{15}$ Pa·s.

3.4. The motion of a plate

We now consider the motion of a plate specifically. From a mathematical point of view, each portion of the lithosphere can be represented as a rigid arc γ on the surface of the Earth. A generic point, p, on the arc has coordinates $-r_{1,p}\hat{u}(\beta_m) + r_{1,s}\hat{u}(\varphi_{1,p})$. Therefore, the first of such points encountered when running counterclockwise (the most westward) is identified by the angle $\varphi_{1,p}$, the last one is identified by the angle $\varphi_{1,p} + 2\alpha$, where $\alpha \in [0, \pi)$ represents the aperture angle associated with the plate, i.e., its angular extent. Given the angular density $\rho = \frac{M_c}{2\alpha}$, we can write the first cardinal equation of dynamics applied to the arc γ in terms of the unknown angle $\varphi_{1,c}$, made by the center of mass c of the rigid body around the center of mass of the Earth. We remark that our equation has an antipodal symmetry. This means that any plate, γ_-, described by the parametric form $(\varphi_{1,a}, \varphi_{1,a} + \pi]$ tends to move as the "opposite" arc γ_+ located at $(-\pi + \varphi_{1,a}, \varphi_{1,a}]$. Since the crust is divided into several plates, so that γ does not coincide with the whole surface of the Earth, the center of mass c is at constant distance form the center of the planet and, therefore, the motion of γ is determined by the motion of c. Hence, we are interested in establishing the equation describing the motion of the plate in terms of $\varphi_{1,c}$. In order to do it, we use the first cardinal equation: the sum of the forces acting on c satisfies

$$M_c \frac{d^2}{dt^2} r_{0,c}\,\hat{u}(\varphi_{0,c}) = F(c) = \int_\gamma F(\varphi_{1,a}) d\,\varphi_{1,a} \tag{21}$$

Considering the lunar tide, the following acceleration is produced:

$$\begin{aligned} a_m(c,e) &:= \frac{1}{M_c}\int_\gamma \frac{f_m(\varphi_{1,a})}{\rho(\varphi_{1,a})} d\,\varphi_{1,a} - \frac{F_m(e)}{M_e} \\ &= \frac{1}{M_c}\int_\gamma \frac{f_m(\varphi_{1,a})}{\rho(\varphi_{1,a})} d\,\varphi_{1,a} - \frac{M_m G}{r_{1,m}^2}\hat{u}(\beta_m) \end{aligned} \tag{22}$$

that can be written, making the calculation at first order in $\lambda_m = \frac{r_{1,p}}{r_{1,m}}$ and recalling $r_{1,a} \equiv r_{1,p}$ for each segment of the plate, as

$$\begin{aligned} a_m(c,e) = 3\,r_{1,p}\Omega_m^2 \frac{\sin\alpha}{\alpha}\cos(\varphi_{1,c} - \beta_m)\,\hat{u}(\beta_m) \\ - \Omega_m^2 r_{1,c}\,\hat{u}(\varphi_{1,c}) \end{aligned} \tag{23}$$

which produces a tangential component of motion following the equation

$$\ddot{\Phi}_c + \frac{3\Omega_m^2}{2}\sin[2(\Phi_c - \gamma t + \beta_m(0))] = 0 \tag{24}$$

where $\Phi_c = -\varphi_{1,c} + \gamma_m t$. A graphical description of the direction and intensity of the accelerating tidal field acting on a rigid plate is provided in Fig. 8. It represents a phase diagram of the effect of lunar and solar earth tides as a function of the position of the Moon and the Sun at time zero. While a completely symmetric force is expected in the case of the classical field for a perfectly elastic Earth, so that the cumulative displacement of the lithosphere with respect to the mantle is zero, the same tidal field acting on an anelastic Earth produces a westerly-oriented motion except for a limited set of astronomical configurations. The point $(0,0)$ corresponds to a situation when the center of mass of the Earth lies on the same straight line joining the center of mass of the Sun and the point p on the surface of the Earth. This is an exceptional configuration. In the real three dimensional space, this corresponds to the Moon crossing the ecliptic plane exactly on the segment joining p and the Sun. In any case, the gravitational outward pull is at its peak. What we have just observed gives an idea of the different degrees of complication in the problem in dimension three. In that case, viewed from Earth, the positions of the Sun and Moon have significantly richer behavior and must be parameterized on the surface of the celestial sphere. This suggests that the measurements of δ and ε must accurately take into account the astronomical configuration at the time of observation. Detailed mathematical derivations are provided in Appendix C.

3.5. Analytical results about the westward drift of the lithosphere

Given the equation of our model for both the Moon and Sun written in explicit form

$$\begin{cases} \ddot{\varphi} + \frac{3\Omega_s}{2}\sin[2(\varphi - q_s - t\gamma_s)] + \frac{3\Omega_m}{2}\sin[2(\varphi - q_m - t\gamma_m)] = 0 \\ \varphi(0) = q,\ \dot{\varphi}(0) = 0 \end{cases} \tag{25}$$

we notice that $\gamma_s \neq \gamma_m$; moreover, ε_s and ε_m are of the same order of magnitude and still greater that the corresponding gravitational constants Ω_s and Ω_m. Formally, if ε_s and ε_m were of the same order of magnitude, considering Moon and Sun separately, would give

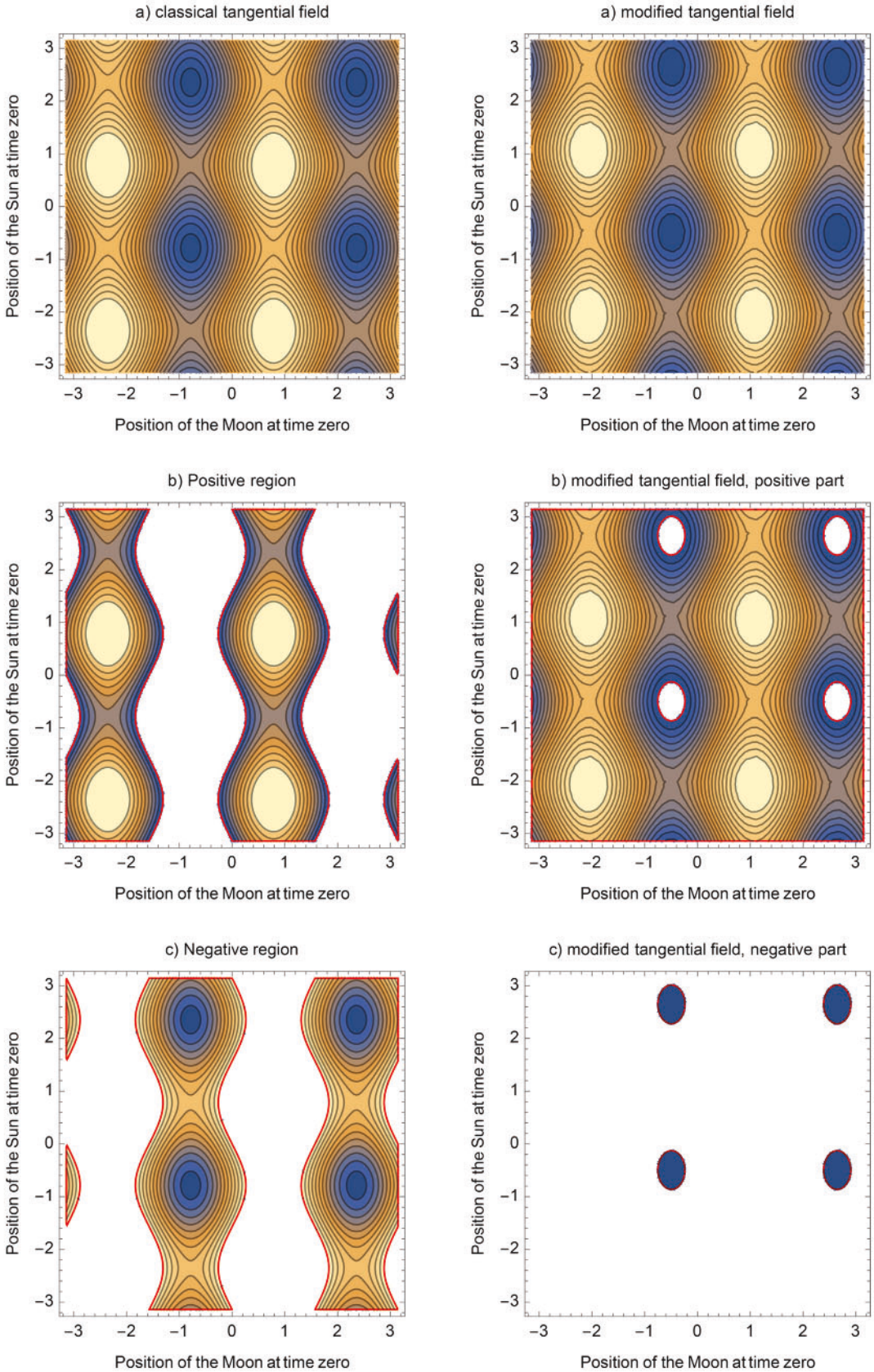

Fig. 8. Phase diagram of level lines describing the direction and intensity of acceleration of the lithosphere produced by the effect of lunar and solar earth tides as a function of the position of the Moon and the Sun at time zero. The left panels represent the classical field for a perfectly elastic Earth, while the right panel shows the same field on a planet with an anelastic component described by a tidal lag angle of $\varepsilon = 1°$. (a) Tangential tidal field. The figure is periodic of period one in this scale in both axes. In the lighter zones the acceleration is westward, in the darkest in eastward. If we do not consider the brake, the maxima and minima are located at points $(\pm 0.25, \pm 0.25)$. (b) The positive part of the tangential tidal field acting to displace the lithosphere to west with respect to the underlying mantle. Notice that almost all the phase space is covered by the a positive tangential tidal field. The red lines are the zero level. (c) The negative part of the tangential tidal field. Notice that the part of the phase space with negative (easterly) drag becomes quite limited in the case of a significant anelastic component in the planetary response to tidal stress. The red lines are the zero level.

$\Omega_m^2 \varepsilon_m \delta_m$ vs $\Omega_s^2 \varepsilon_s \delta_s$; therefore, if only takes just one measure, it could give $\Omega_m^2 \varepsilon_m \delta_m + \Omega_s^2 \varepsilon_s \delta_s$. We do not have a physical reason to take $\delta_s \neq \delta_m$ since they only depend on the mechanical properties of the Earth. So, we have

$$\ddot{\varphi} + K\dot{\varphi} + \frac{3\Omega_m^2}{2} B(\varphi) = 0 \tag{26}$$

We can find an upper estimate of the limit angular velocity for plate motions produced by the drag taking the absolute value of the tidal oscillation

$$\ddot{\varphi}^f + K\dot{\varphi}^f = \frac{3\Omega_m^2}{2}|B(\varphi)| \tag{27}$$

which would lead to

$$\omega \cong \frac{3\Omega_m^2}{2K} \tag{28}$$

For a proof of this formula, see Appendix D. If plates move at the observed velocity, then, the maximum allowed value for the effective viscous coupling between lithosphere and the mantle, K, would satisfy:

$$K \leq K^{\max} := \frac{3\Omega_m^2}{2\omega} \approx 3 \times 10^3 \ s^{-1} \tag{29}$$

where the average westward drift angular velocity is assumed in the order of magnitude of $\omega \approx 3 \times 10^{-16}\ rad\ s^{-1}$. In the linear friction model, the value $K = K^{max}$ cannot be achieved, since it requires a non physical behavior for the force; nevertheless, it can be considered a benchmark. In order to provide a more accurate estimation of friction and plate velocity, we can write

$$K_{\varepsilon,\delta} = \frac{\pi}{2}(\delta\varepsilon) K^{max} \tag{30}$$

where the tidal lag is an angle ε that measures the misalignment of the Moon and Sun with respect to the maximum height of the tidal bulge, the normal decoupling parameter δ is a measure of the ease of lithosphere detachment from asthenosphere. Since $\delta \approx 1$,

$$K_{\varepsilon,\delta} \cong \varepsilon K^{max} \tag{31}$$

represents the limiting case of the previous dynamics in which the Earth's lithosphere is modeled as a thin spherical layer with elevated rigidity except for the boundary of plates in which it is segmented. Therefore, no matter how small the phase delay is, the tidal brake produces, for long times, a westward motion of the lithosphere. In fact, given the model equation

$$\begin{cases} \ddot{\varphi} + K\dot{\varphi} + 3\Omega_m^2 \sin(\varphi - \gamma t)\cos(\varphi - \gamma t)(1-\delta) \\ \qquad = 3\varepsilon\delta\Omega_m^2 [\sin(\varphi - \gamma t)]^2 \\ \varphi(0) = 2q, \quad \dot{\varphi}(0) = 0 \end{cases} \tag{32}$$

it can be written in the equivalent form

$$\begin{aligned} &\ddot{Z} + k_0\dot{Z} + \varepsilon_0\varepsilon^2(1-\delta)\sin[2(Z - t + q)] \\ &\quad = 2\varepsilon_0\varepsilon^3\delta[\sin(Z - t + q)]^2 \end{aligned} \tag{33}$$

where $Z(t) = 2(\Phi(t) - \Phi(0))$; so that, using the homogeneous initial conditions, one gets

$$\begin{aligned} &Z_0 = Z_1 \equiv 0 \\ &\ddot{Z}_2 + k_0\dot{Z}_2 + \varepsilon_0(1-\delta)\sin[2(q-t)] = 0 \\ &\ddot{Z}_3 + k_0\dot{Z}_3 = 2\delta\varepsilon_0[\sin(q-t)]^2 \end{aligned} \tag{34}$$

where Z_2 remains bounded, while Z_3, the dominant term, is linear. Therefore, the limiting angular velocity is furnished by the relationship

$$\lim_{t\to+\infty} \frac{\dot{Z}_3(t)}{t} = \frac{\delta\varepsilon_0}{k_0}\varepsilon^3 \tag{35}$$

which gives

$$\omega = \frac{\delta\lambda}{k_0}\varepsilon \tag{36}$$

So, we have

$$\omega_{\text{plate}} \cong \omega \Longleftrightarrow K := K_{\varepsilon,\delta} \cong \varepsilon\delta K_{\max} \tag{37}$$

This means that our model predicts a westward motion of plates with constant velocity depending on the basal viscosity of the lithosphere and the tidal lag.

4. Discussion

4.1. Mathematical and physical achievements of our model

The causes and extent of the displacement of the surface layer of the lithosphere relative to the underlying mantle have long been debated. One topic considered by many to be controversial is whether gravitational forces are able to contribute appreciably. For the most skeptical, the "westward drift" corresponds to $\omega \approx 0.2°$/Myr, inferred only as a temporary accident related to the faster motion of the Pacific plate being related to the slab pull (e.g., Ricard et al., 1991), being the tidal component irrelevant. Moreover, the literature is poor in estimates about the tidal lag. In our model, we aim to find a mathematical relationship between three potentially measurable physical quantities: the viscosity η, the westward drift velocity with respect to the mantle for long times ω, and the tidal lag ε. To keep the mathematical treatment simple, we treat a two-dimensional model in which Moon and Sun travel their apparent motion with respect to Earth in a single plane. We do not want to hide the fact that the three-dimensional treatment is more complex. But we will not delve into such analysis in this first study. To the best of our knowledge, for the first time the tidal lag ε is included in the model, in a way that appears physically quite natural. Even in this simplified two-dimensional version, an independent theoretical estimation of ε based on the solution of an appropriate free boundary problem does not seem to be known. Our assumptions are as follows. First, the tangential tidal acceleration is restrained in areas where the normal component points toward the Earth's interior as seems unavoidable. This is a very inexpensive way of considering a disconnection parameter, δ. The value of δ is dictated by physical considerations, but could in principle be measured. Second, the peak of the decoupling does not align with the Moon's position, but with the maximum amplitude of the observed solid tide. The exact values of ε are not known. There are various measurements, but the theoretical references to be able to assess their accuracy appear to be uncertain. This will be the subject of future studies. However, we obtain a law that fixes the product of η and ω by constraining it to that of ε. Assuming that ε remains in the range assumed by the most accepted measures, we draw very interesting conclusions. We obtained the following crucial result

$$K\omega = \frac{3(\Omega_m^2 + \Omega_s^2)}{2}\sin\varepsilon = \left(1.9 \times 10^{-13}\sin\varepsilon\right) s^{-2} \tag{38}$$

so that, recalling

$$\omega = \lambda * 5.5 \times 10^{-16}\, rad\ s^{-1}, \quad \varepsilon_0 = \frac{2\pi}{360}, \quad \varepsilon = t_g\varepsilon_0 \tag{39}$$

$\lambda = 1$ corresponds to one degree every million years and $\lambda = 0.1 - 0.2$ would be the most skeptical viewpoint. The value $t_g = 1$ corresponds to a tidal lag of one degree. We have

$$\lambda = \left(\frac{19}{5.5 \times 2.0}\right)\left(\frac{10^{16}}{\eta}\right)\sin\varepsilon \tag{40}$$

and we set here, for the sake of exposition, $t_g = 1$. Then

$$\lambda = \left(\frac{3.0 \times 10^{14}}{\eta}\right)^{\circ}/\text{Myr} \tag{41}$$

We conclude that the values of viscosity completely determine the westward drift velocity according to the above relation, so that, in order to justify the westward drift of the lithosphere, a certain range of minimum basal effective shear viscosity is required: $\eta = 10^{14}, 10^{15}, 10^{16}$ Pa·s respectively imply $\lambda = 3.0^{\circ}$/Myr, 0.3°/Myr, 0.03°/Myr. Therefore, assuming a reasonable tidal angle, of about one degree, and a viscosity approximately equal to the maximums considered, the motion caused solely by the tidal lag would be of the same order of magnitude of what is predicted by the deep hotspot reference frame. This is not the place for a full discussion, but the data above show the power of the Eq. (41). In this concern, excessively low average viscosity seems incomparable with observations of plate motion. In particular, for $\eta = 2 \times 10^{14}$ Pa·s, there would be a westward drift $\omega \approx 1.49^{\circ}$/Myr. This viscosity value would be more than three orders of magnitudes higher than the one inferred by Jordan (1974). Moreover, it is consistent with the presence of partial melting in the LVZ (Panza et al., 2010; Hua et al., 2023), confirming the ultra-low viscosity (10^{12} Pa·s) obtained by experimental results and inferred to occur in the LVZ (Jin et al., 1994; Stevenson, 1994). This wide viscosity range easily allows to compute a velocity of the westerly drift faster than $\omega > 1^{\circ}$/Myr driven by the tidal torque, confirming a full westerly rotation of the lithosphere relative to the underlying mantle along the tectonic equator (Doglioni and Panza, 2015).

4.2. Geodynamic consequences of our model

The Earth showcases a certain degree of anelasticity in the mechanical response to tides. When the Moon or the Sun are at their own zenith, the surface protrudes with a short delay, producing a misaligned bulge with respect to the line of maximum Earth-Moon gravitational attraction (Munk, 1997). The tidal lag can be theoretically estimated (Goldreich and Soter, 1966) by

$$\varepsilon = \arctan\left[\frac{1}{4\pi E}\oint\left(-\frac{dE}{dt}\right)dt\right] \tag{42}$$

where E is the maximum potential energy accumulated during by the tidal strain, while the quantity $-\frac{dE}{dt}$ represents the loss rate of energy dissipated during a tidal cycle. Hence, the larger the tidal lag, the larger the dissipated energy, which is in agreement with our model and the previous paragraph in particular (compare with Eq. (37)). The physical properties of the Earth produce a lag angle of $\varepsilon \sim (0.3 - 2.4)^{\circ}$. Such misalignment is due to the combined effect of three different processes: the different response of the Solid and Liquid Earth to the tidal perturbation, being the displacement of fluids slower than that of rocks, producing a loading on the ocean bathimetry; the torque determined by the asymmetric position of the Earth-Moon center of gravity and the global anelasticity of the planet. Therefore, tides can slower the Earth's rotational velocity so that the length of day increases about 2.3 ms/century. This explains why about 400 million years ago each year was made up of about 400 days since a day lasted about 20 h. Moreover, the tidal torque on the Earth produced by the Sun and the Moon can be written as

$$M_t \sim \frac{9Gr_e^5}{4}\left[\frac{m_m^2}{d_{e,m}^6\left(1+\frac{19\mu_m}{2g\rho_m r_e}\right)} + \frac{m_s^2}{d_{e,s}^6\left(1+\frac{19\mu_s}{2g\rho_s r_e}\right)}\right]\sin(2\epsilon) \tag{43}$$

where μ_m and μ_s stand respectively for the average rigidity of the Moon and Sun and r_e is the Earth's radius. A significant portion of the torque above is dissipated within the upper mantle, about $\Delta M \sim \frac{2}{3}M_t$. Such differential torque dissipates about 2×10^{20} J/yr; such amount is several times larger than the energy released each year by the earthquakes all over the world; therefore, even though only a little part of it was dissipated in the upper mantle, the energy budget for allowing a westward oriented motion of the lithosphere will be available (Bostrom, 1971; Doglioni, 1990; Verard et al., 2012). However, the torque needed for keeping a differential rotation of angular velocity ω between concentric spheres inside the Earth with different viscous rheology in a homogeneous mantle at rest is given by about $M_{drag} \approx 10^3\,\eta\,N \cdot m$ (Jordan, 1974); therefore, according to this calculation, tides could be able to speed up plate motions only if the effective shear viscosity $\eta \leq 10^{13}$ Pa·s, while a significant long-term modulation of plate motion is possible up to $\eta \leq 10^{16}$ Pa·s. This is the reason why the astronomical, i.e., tidal forces have been mostly discarded so far in the modeling of plate tectonics: the high viscosity (10^{19} Pa·s) inferred in the asthenosphere, in particular by glacial isostatic adjustment (e.g., Mitrovica and Forte, 2004; Cathles, 2015) is too high to allow a significant role for tidal forces in plate tectonics. However, thin low-viscosity layers are invisible to several routinely techniques, and much lower viscosity values (10^{12-15} Pa·s) have been reported by mineropetrological studies (e.g., Jin et al., 1994; Hirth and Kohlstedt, 1995). A viscosity of 10^{17} Pa·s was computed using the remote triggering of earthquakes (Pollitz et al., 1998). Moreover, viscosity under a vertical load is much higher with respect to the horizontal shear, especially if water or some melting occurs in the asthenosphere (Scoppola et al., 2006). In addition, Carcaterra and Doglioni (2018) showed that the average value of viscosity of the upper mantle is not a crucial quantity for geodynamic purposes. The dominant term affecting the westward drift of the lithosphere hypothetically produced by tidal drag depends on the minimal value of viscosity. In literature, the minimum values of the asthenospheric viscosity are usually assumed to be in the order of $\eta_{min} \sim 10^{18}$ Pa·s (Cathles, 2015) or even lower as a consequence of post-seismic relaxation (e.g., Qiu et al., 2018) or below oceanic plates featured by $\eta_{min} \geq 10^{17}$ Pa·s, (e.g., Pollitz et al., 1998; Becker, 2017). Moreover, investigating the hypothesis on which the above calculation is grounded on, the mantle is neither homogeneous nor it is at rest, but, at least in its upper part, is vigorously convecting due to the high thermal gradient at the asthenosphere top. Based on petrologic and physical constraints, Anderson postulated that deep mantle convection should be very slow and sluggish, favoring a recycling driven from the top and inhibiting the surficial return of deep mantle material due to the irreversible stratification of the mantle (Anderson, 2001; Anderson, 2002). The decoupling at the low-velocity zone between 100–200 km depth at the lithosphere-asthenosphere interface, is a consequence of the net rotation of the lithosphere (Ricard et al., 1991; Gripp and Gordon, 2002; Crespi et al., 2007), that is moving westerly relative to the hotspots, but also consistent with the low-velocity layer recorded by absolute tomography images of the upper mantle (Thybo, 2006; Panza et al., 2010) and magnetotelluric surveys measuring mantle resistivity (Naif et al., 2013). A decoupling at the lithosphere-asthenosphere boundary is consistent with the strong viscosity contrast up to 8–10 orders of magnitude (Doglioni et al., 2011) and inferred from deep seismic reflection technique (Audhkhasi and Singh, 2022). Weismüller et al. (2015) by means of geodynamic simulations postulated a decollement and vigorous asthenospheric convection with a relative flow at least one order of magnitude faster than the overlying tectonic plates. On the other side, several models of mantle convection have been proposed during the last decades

(see Coltice et al., 2017 for a review). However, the volumes consumed along tthe W-directed subduction zones are far larger than those along tthe opposite slabs, supporting an asymmetric mantle convection (Doglioni and Anderson, 2015; Ficini et al., 2020). Moreover, Bullen (1940), Birch (1952), Bunge (2005), Anderson (2013) have demonstrated a fundamental issue of the Earth's mantle, i.e., most of it is in subadiabatic condition. A potential temperature lower than the adiabatic prevents active upwelling of the mantle and convection. This is one of the reasons why plate tectonics and mantle convection seem to be rather generated by a top-down driving mechanism rather than bottom up (Anderson, 2001). Being the top asthenosphere (i.e., the LVZ) in superadiabatic temperature, it can convect much faster than the underlying mantle, drastically decreasing the viscosity,hence providing a mechanical decoupling. Notice that the thermal gradient in the LVZ, between 100–200 km depth can be up to 3°C/km, whereas the underlying mantle can be about 0.4°C/km. Water content, pargasitic amphibolite breakdown (Green et al., 2010), high temperature and relative lower pressure can determine higher Rayleigh number, i.e., more efficient convection, lower viscosity and consequent decoupling. This may allow the decoupling of the overlying lithosphere dragged by solid Earth's tides. However, the results about tidal drag and mantle viscosity are only marginally compatible with a role of the tidal torque in geodynamics, which is however suggested by several geological, geophysical and geochemical evidences described in the introduction. A value of viscosity of $\eta \leq 10^{16}$ Pa·s is still required to permit a tectonic plate drift speed of about some centimeters per year, even though there is evidence that the viscosity of the asthenosphere may be overestimated, above all on the light of a stronger and stronger evidence of a globally prevalent partial melting diffuse within the low velocity zone (e.g., Hua et al., 2023). Recalling the hypothesis of the calculation of the differential torque required to allow the mechanical decoupling between lithosphere and asthenosphere, the upper mantle is considered to be at rest and the total work is thought to be furnished by tidal forces. This assumption is not reasonable. Even though stratified, convection certainly occurs in the upper mantle. This additional contribution may reconcile our observations with previous scientific literature. In addition, differential rotation between convecting concentric layers implies transfer of angular momentum, so that fluids flow to maximize it (Běhounková et al., 2010; Ogilvie and Lesur, 2012; Mannix and Mestel, 2021). This property is also supported by experimental evidence. So, differential rotation is, in principle, able to polarize mantle convection, which turns out to be top-down controlled, as suggested in Anderson (2001). Seismic anisotropy can be considered as an evidence of this effect: in the shallower layers of the upper convecting mantle, crystals are oriented along the direction of maximum stress produced by the differential velocity between the lithosphere and the asthenosphere. Therefore, on the base of the output of our model, numerical simulations and geological data, we suggest that the large-scale, widespread evidence of polarized plate tectonics may be allowed by a combination of stratified and top-down-polarized mantle circulation in the upper mantle, providing part of the lacking torque required by the Jordan's calculation, and the direct effect of tidal drag of the lithosphere. Our model also confirms that, while high-frequency tidal harmonics (bi-weekly and monthly tides, the semi-annual and annual terms) cannot modulate plate motions, some significant long-period tides (e.g., the polar and the 18.6-years-long period tide, compare with Fig. 9) can do it (Fig. 7). This result is compatible with the conclusions reported in Zaccagnino et al. (2020). The nominal and observed amplitudes are well reproduced if a basal viscosity of the lithosphere is assumed in the range of $10^{15} \leq \eta \leq 10^{16}$ Pa·s, which also results in agreement with a westward drift of the lithosphere ($\omega \approx 0.1° - 0.3°$/Myr). On the other side, short period tides can instead modulate plate motions indirectly along weak plate margins, such as subduction zones, triggering silent events and moderate seismicity, e.g., Cochran et al. (2004); Ide and Tanaka (2014); Zaccagnino et al. (2022), according to the different mechanisms described in Scholz et al. (2019); Varga and Grafarend (2019); Zaccagnino et al. (2022). However, a lower value of viscosity under shear can easily allow an even larger decoupling between the lithosphere and the asthenosphere; hence, a faster westward drift up to $\omega \approx 1.49°$/Myr, which is the value predicted by the shallow hotspot reference frame (SHRF) of Doglioni et al. (2005), with $\eta \approx 2 \times 10^{14}$ Pa·s.

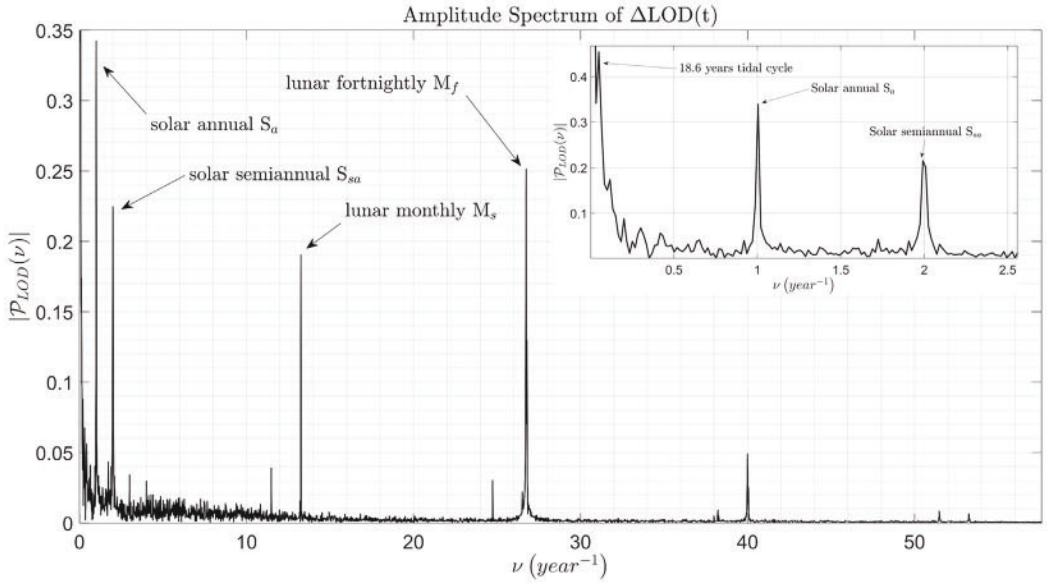

Fig. 9. Fast Fourier Transform of the variations of the length of day Δ LOD (1962–2022). Tidal frequencies dominate the spectrum. Tides are responsible of large part of the oscillations of Δ LOD. Minor contributions at higher frequencies are due to recurrent atmospheric and ocean circulation.

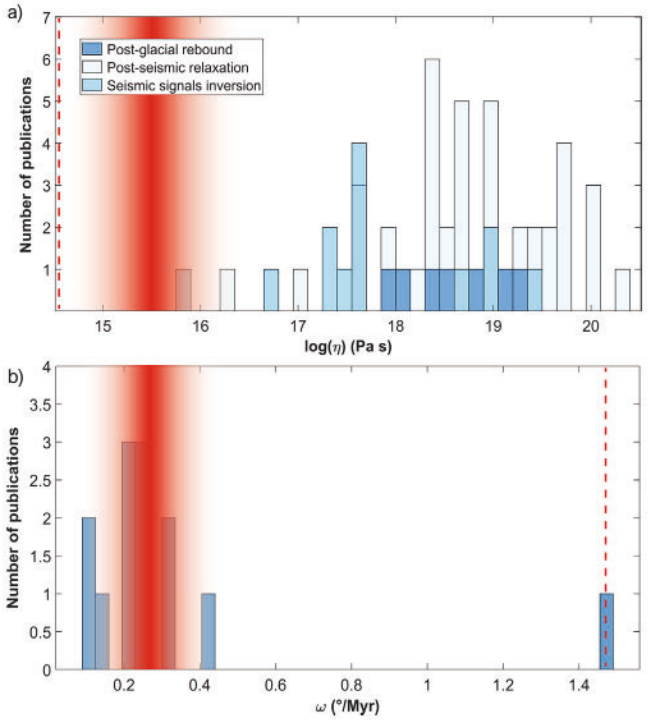

Fig. 10. Comparison between data published in scientific literature and predictions of our model. In the present paper is shown that a westward drift of the lithosphere with angular velocity $\omega \approx 0.1° - 0.3°$/Myr (deep hotspot reference frame) is compatible with a basal effective viscosity computed under shear $\eta \approx 10^{15} \div 10^{16}$ Pa·s (red shadows), while $\omega \approx 1.49°$/Myr (shallow hotspot reference frame) requires an average effective viscosity computed under shear $\eta \approx 2 \times 10^{14}$ Pa·s (red dashed lines). Data from Knopoff and Leeds, 1972; Ricard et al., 1991; Pollitz et al., 1998; Ranalli, 2000; Gripp and Gordon, 2002; Cuffaro and Doglioni, 2007; Conrad and Behn, 2010; Wang, 2010; Torsvik et al., 2010; Höink et al., 2011; Cathles, 2015; Becker, 2017; Chanard et al., 2018; Qiu et al., 2018; Pollitz, 2019.

5. Conclusions

Global geodynamics undergoes the effect of several stress sources of different origin such as plate boundary forces, mantle motions, which are usually considered to be dominant in driving plate tectonics. However, evidence exists that these mechanisms are not sufficient to explain large-scale lithosphere dynamics. Plates follow a westward mainstream and the lithosphere with long-term angular velocity of about $\omega \approx 0.1° - 0.3°$/Myr relative to the underlying mantle in the deep hotspot reference frame, which may increase up to $\omega \approx 1.0° - 1.5°$/Myr according to the shallow hotspot reference frame model. Such asymmetry, together with other geophysical and geological observations suggest an exogenous contribution to plate tectonics. Nevertheless, the torque provided by tidal forces is usually considered too weak to directly speed up plates. However, the interaction between the stratified mantle convection, the ultra-low viscosity within the Low Velocity Zone (LVZ) atop the asthenosphere and solid Earth tides could explain why plate tectonics appears to be westerly polarized. In this work, we propose a mathematical model to address this issue providing both analytical results and computational simulations. We show that the tidal drag allows to explain why absolute plate motions, regardless of the reference frame, show a significant west-ward drift of the lithosphere with respect to the underlying mantle while the variability of angular velocity among plates is controlled by the basal viscosity at the interface between the lithosphere and the mantle. Our results suggest that a westward drift of the lithosphere with angular velocity $\omega \approx (0.1 - 0.3)°$/Myr can be justified by a basal effective viscosity under shear $\eta \approx 10^{15} \div 10^{16}$ Pa·s (Fig. 6), which is also compatible with the millimetric low-frequency (period $\geq 10^9$ s, compare with Fig. 9) tidal modulations of plate motions. In fact, while high frequency tides do not affect plate velocity, i.e., they only produce an elastic response of the Earth, our simulations show small, but significant viscoelastic tidal modulations of plate motions with respect to the deep mantle (Fig. 7), coherent with the GNSS measurements in long-lasting

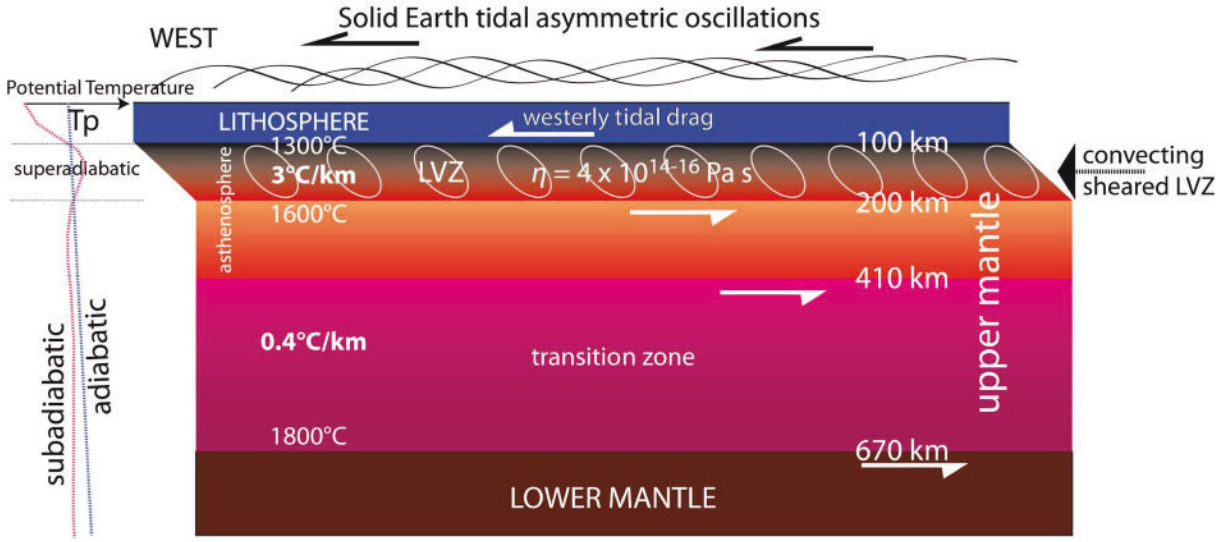

Fig. 11. Convection in the upper mantle is allowed by super-adiabatic thermal conditions and constrained by petrological stratification. Low viscosity, rheological heterogeneities and stratified convection allow the decoupling of the lithosphere from the underlying layers under the action of the tidal drag. Most of the mantle is inferred to be in sub-adiabatic condition, preventing large scale and vigorous active convection. Super-adiabatic mantle potential temperatures are rather inferred only atop asthenosphere, i.e., the low-velocity zone (LVZ), where mantle convection can be very efficient, allowing the decoupling of the lithosphere driven from the top, i.e., by the tidal drag. Therefore, solid Earth tides may provide the energy to westerly shift the lithosphere, whereas the asthenosphere small scale convection allows lowering of the effective viscosity and the decoupling with the overlying plates. Notice the almost ten times higher thermal gradient in the LVZ with respect to the underlying upper mantle.

time series compatible with the output of the analysis reported in Zaccagnino et al. (2020). Lower values of viscosity may allow an even larger decoupling between the lithosphere and the asthenosphere; hence, faster westward drift up to $\omega \approx 1.49°$/Myr proposed in Doglioni et al. (2005) and in Cuffaro and Doglioni (2007) if $\eta \approx 2 \times 10^{14}$ Pa·s. While our conclusions about the rate of the westward drift of the lithosphere is compatible with previous literature, the value of basal viscosity of the low velocity zone under shear is about three order of magnitude lower than the average measures obtained with different methods (Fig. 10). It is worthy to notice that a thin very low viscosity layer may have been missed because of the limited resolving power of the techniques correctly applied for the estimation of viscosity, which are more tuned to unravel average viscosity over relatively large thicknesses. However, recently, growing evidence has been collected suggesting the presence of thin (few kilometers-thick) ultra-low viscosity layers, e.g., Audhkhasi and Singh (2022); Hua et al. (2023). We also explain such difference on the light of a possible contribution to lithosphere-asthenosphere decoupling due to polarized convection and nonlinear viscous behavior of the upper mantle. The final picture of our model is graphically represented in Fig. 11. Furthermore, the effective viscosity of the weakest layers at the base of lithosphere may be still overestimated by the methods currently used for inference. This possibility should be considered on the light of the growing evidence of diffuse melt fraction in the upper asthenosphere.

CRediT authorship contribution statement

Vincenzo Nesi: Conceptualization, Formal analysis, Investigation, Methodology, Software, Validation, Visualization, Writing - original draft, Writing - review & editing. **Oscar Bruno**: Conceptualization, Formal analysis, Investigation, Methodology, Validation. **Davide Zaccagnino**: Conceptualization, Investigation, Validation, Visualization, Writing - original draft, Writing - review & editing. **Corrado Mascia**: Conceptualization. **Carlo Doglioni**: Conceptualization, Funding acquisition, Project administration, Supervision, Visualization, Writing - review & editing.

Declaration of Competing Interest

The authors declare that they have no known competing financial interests or personal relationships that could have appeared to influence the work reported in this paper.

Acknowledgements

The authors are grateful to a long list of colleagues who provided constructive criticism to the research. Vincenzo Nesi gratefully acknowledges support from Progetto di Ricerca 2020, Progetto di Ricerca di Ateneo 2021, "Equazioni differenziali ellittiche e paraboliche non lineari" Sapienza n. RM120172B8F74615; Oscar Bruno gratefully acknowledges support from NSF under contract DMS-2109831, from AFOSR under contract FA9550-21-1–0373, and from the NSSEFF Vannevar Bush Fellowship under ONR contract number N00014-16–1-2808; The research was also supported by ESA grant 4000133529/20/NL/GP (Doglioni).

Appendix A. Parameters and symbols

Below we list the symbols and parameters appearing in the mathematical derivation of results:

- $T_D \cong$ period of the diurnal tidal harmonics;
- $T_M \cong$ period of the monthly lunar harmonics;
- $T_S \cong$ one year;
- m_m = Moon's mass;
- $d_{e,m}$ = Lunar distance;
- $\Omega_m^2 = \frac{Gm_m}{(d_{e,m})^3}$;
- G = Gravitational constant;
- $\gamma_m = \frac{2\pi}{T_D} - \frac{2\pi}{T_M}$;
- ε_m = Lunar tidal lag angle;
- q = initial position of the particle;
- q_m = initial position of the Moon;
- q_s = initial position of the Sun;
- m_s = Sun's mass;
- $d_{e,s}$ = Solar distance;
- $\Omega_s^2 = \frac{Gm_s}{(d_{e,s})^3}$;
- $\gamma_s = \frac{2\pi}{T_D} - \frac{2\pi}{T_S}$;
- ε_s = Solar tidal lag angle;
- δ_s = Sun tidal brake;
- δ_m = Moon tidal brake;
- φ = parameter describing the relative position of the celestial body and the Earth in the inertial system.
- $\Phi = -\varphi + \gamma t$.
- $\beta_m(t) = \gamma_m t + \beta_m(0)$ spatial parameter describing the Moon's position.
- $\beta_s(t) = \gamma_s t + \beta_s(0)$ spatial parameter describing the Sun's position.
- $\lambda = \frac{3\Omega_m^2}{4\gamma^2} \cong 0.6 \times 10^{-5}$.
- Additional auxiliary variables used in calculations

$$c_m^2 = \frac{3\Omega_m^2(1-\delta_m \cos\varepsilon_m)}{2}, \qquad c_s^2 = \frac{3\Omega_s^2(1-\delta_s \cos\varepsilon_s)}{2}$$
$$d_m^2 = 3\Omega_m^2 \delta_m \sin\varepsilon_m, \qquad d_s^2 = 3\Omega_s^2 \delta_s \sin\varepsilon_s \tag{A.1}$$

$$L_m(t) = l_m(t) - h_m, \quad L_s(t) = l_s(t) - h_s \tag{A.2}$$

Appendix B. Reference systems

We consider three two-dimensional coordinate systems in our work: an inertial one centered at the center of the Sun, a second one with origin at the center of the Earth and with axes parallel to those of the inertial one, and a third coordinate system, with the same center of the second, but rotating with the Earth. In polar coordinates, the position of a point in a two-dimensional system in the aforementioned reference frames is given by

$$\vec{r}_{0,p} = r_{0,p}\,\hat{u}(\varphi_{0,p}),\ \vec{r}_{1,p} = r_{1,p}\,\hat{u}(\varphi_{1,p}),\ \vec{r}_{2,p} = r_{2,p}\,\hat{u}(\varphi_{2,p}) \tag{B.1}$$

respectively. The arguments of the unit vectors $\hat{u}$ are angles counted counterclockwise. The angles $\varphi_{0,p}$ and $\varphi_{1,p}$ are those formed by the vectors $\vec{r}_{0,p}$ and $\vec{r}_{1,p}$ with respect to a horizontal line. By definition

$$\varphi_{1,p} = \varphi_{2,p} + \frac{2\pi}{T_D} t \tag{B.2}$$

where T_D is the time the Moon spends in its apparent daily motion around the Earth so that $t \to R(t) = \frac{2\pi}{T_D} t$ parameterizes the angle measuring the rotation of the Earth around its axes.

Appendix C. Mathematical modeling of the motion of a plate

The center of mass of a plate, according to the preliminary description provided in paragraph 3.4, γ, defined by c is given by

$$c = \frac{M_c}{2\delta M_c}\left(-r_{1,s}\hat{u}(\beta_s)\,2\delta + \int_\gamma r_{1,q}\hat{u}(\varphi_{1,q})\,d\varphi_{1,q}\right). \tag{C.1}$$

Hence, recalling that $r_{1,a} = r_{1,p}$, we have

$$c + r_{1,m}\,\hat{u}(\beta_m) = \frac{r_{1,p}}{2\alpha}\int_{\varphi_{1,a}}^{\varphi_{1,a}+2\alpha} \hat{u}(\varphi_{1,a})\,d\varphi_{1,a}. \tag{C.2}$$

The vector to integrate $\hat{u}(\varphi_{1aq})$, admits the explicit primitive $-\hat{u}^{\perp}(\varphi_{1,a})$. Hence

$$c + r_{1,m}\,\hat{u}(\beta_m) = -\frac{r_{1,p}}{2\alpha}(\hat{u}^{\perp}(\varphi_{1,p}+2\alpha) - \hat{u}^{\perp}(\varphi_{1,p})) \tag{C.3}$$

and setting

$$\varphi_{1,p} + \alpha = \varphi_{1,c} \tag{C.4}$$

we obtain

$$\begin{aligned} c + r_{1,m}\,\hat{u}(\beta_m) &= -\frac{r_{1,p}}{2\alpha}(\hat{u}^{\perp}(\varphi_{1,c}+\alpha) - \hat{u}^{\perp}(\varphi_{1,c}-\alpha)) \\ &= r_{1,p}\,\frac{\sin\alpha}{\alpha}\,\hat{u}(\varphi_{1,c}). \end{aligned} \tag{C.5}$$

Therefore, defining $r_{1,c} = r_{1,p}\frac{\sin\alpha}{\alpha}$, $\varphi_{1,c} = \varphi_{1,p} + \alpha$, we finally get:

$$c = r_{1,c}\,\hat{u}(\varphi_{1,c}) - r_{1,m}\,\hat{u}(\beta_m). \tag{C.6}$$

Since the crust is divided into several plates, so that γ does not coincide with the whole surface of the Earth, the center of mass c is at constant and positive distance form the center of the planet and therefore is motion of γ is determined by the motion of c. Hence, we are interested in establishing the equation describing the motion of the plate in terms of $\varphi_{1,c}$. In order to do it, we use the first cardinal equation: the sum of the forces acting on c satisfies

$$M_c\,\frac{d^2}{dt^2} r_{0,c}\,\hat{u}(\varphi_{0,c}) = F(c) = \int_{\gamma} F(\varphi_{1,a})\,d\varphi_{1,a}. \tag{C.7}$$

Therefore

$$\frac{d^2}{dt^2}\left(r_{0,c}\,\hat{u}(\varphi_{0,c}) - r_{0,e}\,\hat{u}(\varphi_{0,e})\right) = \frac{F(c)}{M_c} - \frac{F(e)}{M_e}. \tag{C.8}$$

To compute the right hand side, we consider the density of the gravitational forces acting on the plate, $f_m(\varphi_{1,a})$ produced by the lunar perturbation, which determines the following acceleration:

$$\begin{aligned} a_m(c,e) &:= \frac{1}{M_c}\int_{\gamma}\frac{f_m(\varphi_{1,a})}{\rho(\varphi_{1,a})}\,d\varphi_{1,a} - \frac{F_m(e)}{M_e} \\ &= \frac{1}{M_c}\int_{\gamma}\frac{f_m(\varphi_{1,a})}{\rho(\varphi_{1,a})}\,d\varphi_{1,a} - \frac{M_m G}{r_{1,m}^2}\,\hat{u}(\beta_m). \end{aligned} \tag{C.9}$$

For the sake of simplicity, we make the calculation at first order in $\lambda_m = \frac{r_{1,p}}{r_{1,m}}$ and recall that $r_{1,a} \equiv r_{1,p}$ for each segment of the plate; so we have

$$\frac{1}{\left\|-r_{1,m}\,\hat{u}(\beta_m) + r_{1,p}\,\hat{u}(\varphi_{1,a})\right\|^3} \cong \frac{1 + 3\,\lambda_m\cos(\varphi_{1,a}-\beta_m)}{r_{1,m}^3},$$

so that

$$\begin{aligned} a_m(c,e) &\cong -\frac{M_m G}{M_c r_{1,m}^3}\int_{\gamma}\rho(\phi_{1,a})\,(1+3\,\lambda_m\cos(\varphi_{1,a}-\beta_m))\,(-r_{1,m}\,\hat{u}(\beta_m) \\ &\quad + r_{1,a}\,\hat{u}(\varphi_{1,a}))\,d\varphi_{1,a} - \frac{M_s G}{r_{1,m}^2}\,\hat{u}(\beta_m) \\ &= -\frac{M_m G}{2\alpha\, r_{1,m}^3}\int_{\gamma}(1+3\,\lambda_m\cos(\varphi_{1,a}-\beta_m))\,(-r_{1,m}\,\hat{u}(\beta_m) \\ &\quad + r_{1,a}\,\hat{u}(\varphi_{1,a}))\,d\varphi_{1,a} - \frac{M_m G}{r_{1,m}^2}\,\hat{u}(\beta_m) \\ &= \frac{3\,r_{1,p}\Omega_m^2}{2\alpha}\left(\int_{\gamma}\cos(\varphi_{1,a}-\beta_m)\,d\varphi_{1,a}\right)\hat{u}(\beta_m) \\ &\quad - \Omega_m^2\left(\frac{r_{1,p}}{2\alpha}\int_{\gamma}\hat{u}(\varphi_{1,a})\,d\varphi_{1,a}\right). \end{aligned} \tag{C.10}$$

Recall that

$$\begin{aligned} \frac{1}{2\alpha}\int_{\gamma} r_{1,a}\,\hat{u}(\varphi_{1,a})\,d\varphi_{1,a} &= \frac{r_{1,p}}{2\alpha}\int_{\varphi_{1,p}}^{\varphi_{1,p}+2\alpha}\hat{u}(\varphi_{1,a})\,d\varphi_{1,a} \\ &= r_{1,p}\,\frac{\sin\alpha}{\alpha}\,\hat{u}(\varphi_{1,c}) = r_{1,c}\,\hat{u}(\varphi_{1,c}). \end{aligned} \tag{C.11}$$

It follows

$$\begin{aligned} a_s(c,e) &= \frac{3\,r_{1,p}\Omega_m^2}{2\alpha}\left(\int_{\gamma}\cos(\varphi_{1,a}-\beta_m)\,d\varphi_{1,a}\right)\hat{u}(\beta_m) \\ &\quad - \Omega_m^2\,r_{1,c}\,\hat{u}(\varphi_{1,c}) \end{aligned} \tag{C.12}$$

$$\begin{aligned} a_s(c,e) &= \frac{3\,r_{1,p}\Omega_m^2}{2\alpha}\,[\sin(\varphi_{1,c}-\beta_m+\alpha) - \sin(\varphi_{1,c}-\beta_m \\ &\quad - \alpha)]\,\hat{u}(\beta_m) - \Omega_m^2\,r_{1,c}\,\hat{u}(\varphi_{1,c})]. \end{aligned} \tag{C.13}$$

Now recall that

$$\begin{aligned} &\sin(\varphi_{1,c}-\beta_m+\alpha) - \sin(\varphi_{1,c}-\beta_m-\alpha) \\ &\quad = 2\cos(\varphi_{1,c}-\beta_s)\sin\alpha. \end{aligned} \tag{C.14}$$

Thus

$$\begin{aligned} a_m(c,e) &= 3\,r_{1,p}\Omega_m^2\,\frac{\sin\alpha}{\alpha}\cos(\varphi_{1,c}-\beta_m)\,\hat{u}(\beta_m) \\ &\quad - \Omega_m^2\,r_{1,c}\,\hat{u}(\varphi_{1,c}) \\ &= r_{1,c}\Omega_m^2\left(3\cos(\varphi_{1,c}-\beta_m)\hat{u}(\beta_m) - \hat{u}(\varphi_{1,c})\right). \end{aligned} \tag{C.15}$$

Using (C.15) we get

$$\begin{aligned} &r_{1,c}\,(\ddot{\varphi}_{1,c}\,\hat{u}^{\perp}(\varphi_{1,c}) - \dot{\varphi}_{1,c}^2\,\hat{u}(\varphi_{1,c})) \\ &\quad = r_{1,c}\Omega_m^2(3\cos(\varphi_{1,c}-\beta_m)\,\hat{u}(\beta_m) - \hat{u}(\varphi_{1,c})). \end{aligned} \tag{C.16}$$

The tangential component gives

$$\begin{aligned} \ddot{\varphi}_{1,c} &= -\Omega_m^2\,(3\cos(\varphi_{1,c}-\beta_m)\,\sin(\varphi_{1,c}-\beta_m)) \\ &= -\frac{3\,\Omega_m^2}{2}\sin[2\,(\varphi_{1,c}-\beta_m)], \end{aligned} \tag{C.17}$$

hence

$$\ddot{\varphi}_{1,c} + \frac{3\Omega_m^2}{2}\sin[2\,(\varphi_{1,c}-\beta_m)] = 0, \tag{C.18}$$

i.e., setting $\Phi_c = -\varphi_{1,c} + \gamma t$,

$$\ddot{\Phi}_c + \frac{3\Omega_m^2}{2}\sin[2\,(\Phi_c - \gamma t + \beta_m)] = 0. \tag{C.19}$$

Appendix D. Proof of the limit angular velocity

Mathematically, one can prove

$$\omega_{\infty}^f \cong \frac{3\Omega_m^2}{2K} \tag{C.20}$$

by using the Gronwall's Lemma. Indeed, by Eq. (27), one has

$$\frac{1}{e^{-Kt}}\frac{d}{dt}(e^{Kt}\dot{\varphi}^f) \le \frac{3\Omega_m^2}{2} \tag{C.21}$$

Integrating in time and using the initial conditions one has

$$\dot{\varphi}^f \le \frac{3\Omega_m^2}{2K}(1 - e^{-Kt}) \le \frac{3\Omega_m^2}{2K} \tag{C.22}$$

References

Agnew, D., 2010. 6 - earth tides. Treatise Geophys. 3, 163.

Anderson, D., 2013. The persistent mantle plume myth. Aust. J. Earth Sci. 60, 657–673.

Anderson, D.L., 2001. Top-down tectonics? Science 293, 2016–2018.

Anderson, D.L., 2002. The case for irreversible chemical stratification of the mantle. Int. Geol. Rev. 44, 97–116.

Audhkhasi, P., Singh, S.C., 2022. Discovery of distinct lithosphere-asthenosphere boundary and the Gutenberg discontinuity in the Atlantic ocean. Sci. Adv. 8, eabn5404.

Becker, T.W., 2017. Superweak asthenosphere in light of upper mantle seismic anisotropy. Geochem. Geophys. Geosyst. 18, 1986–2003.

Běhounková, M., Tobie, G., Choblet, G., Čadek, O., 2010. Coupling mantle convection and tidal dissipation: Applications to enceladus and earth-like planets. J. Geophys. Res.: Planets 115, E09011.

Birch, F., 1952. Elasticity and constitution of the Earth's interior. J. Geophys. Res 57, 227–286.

Bonatti, E., 1990. Not so hot hot spots in the oceanic mantle. Science 250, 107–111.

Bostrom, R., 1971. Westward displacement of the lithosphere. Nature 234, 536–538.

Bullen, K., 1940. The problem of the earth's density variation. Bull. Seismol. Soc. Am. 30, 235–250.

Bunge, H.P., 2005. Low plume excess temperature and high core heat flux inferred from non-adiabatic geotherms in internally heated mantle circulation models. Phys. Earth Planet. Inter. 153, 3–10.

Carcaterra, A., Doglioni, C., 2018. The westward drift of the lithosphere: A tidal ratchet? Geosci. Front. 9, 403–414.

Cathles, L.M., 2015. Viscosity of the Earth's Mantle, volume 1362. Princeton University Press.

Chanard, K., Fleitout, L., Calais, E., Barbot, S., Avouac, J.P., 2018. Constraints on transient viscoelastic rheology of the asthenosphere from seasonal deformation. Geophys. Res. Lett. 45, 2328–2338.

Cochran, E.S., Vidale, J.E., Tanaka, S., 2004. Earth tides can trigger shallow thrust fault earthquakes. Science 306, 1164–1166.

Coltice, N., Gérault, M., Ulvrová, M., 2017. A mantle convection perspective on global tectonics. Earth Sci. Rev. 165, 120–150.

Conrad, C.P., Behn, M.D., 2010. Constraints on lithosphere net rotation and asthenospheric viscosity from global mantle flow models and seismic anisotropy. Geochem. Geophys. Geosyst. 11(5), Q05W05.

Crespi, M., Cuffaro, M., Doglioni, C., Giannone, F., Riguzzi, F., 2007. Space geodesy validation of the global lithospheric flow. Geophys. J. Int. 168, 491–506.

Cuffaro, M., Caputo, M., Doglioni, C., 2008. Plate subrotations. Tectonics 27 (4), TC4007.

Cuffaro, M., Doglioni, C., 2007. Global kinematics in deep versus shallow hotspot reference frames. Special Papers-Geological Soc. Am. 430, 359.

Doglioni, C., 1990. The global tectonic pattern. J. Geodyn. 12, 21–38.

Doglioni, C., 1992. Main differences between thrust belts. Terra Nova 4, 152–164.

Doglioni, C., 1993. Geological evidence for a global tectonic polarity. J. Geological Soc. 150, 991–1002.

Doglioni, C., Anderson, D.L., 2015. Top-driven asymmetric mantle convection. The Interdisciplinary Earth: A Volume in Honor of Don L. Anderson, 51–63.

Doglioni, C., Carminati, E., Cuffaro, M., Scrocca, D., 2007. Subduction kinematics and dynamic constraints. Earth Sci. Rev. 83, 125–175.

Doglioni, C., Green, D.H., Mongelli, F., 2005. On the shallow origin of hotspots and the westward drift of the lithosphere. Geolog. Soc. Am. Special Papers 388, 735–749.

Doglioni, C., Ismail-Zadeh, A., Panza, G., Riguzzi, F., 2011. Lithosphere–asthenosphere viscosity contrast and decoupling. Phys. Earth Planet. Inter. 189, 1–8.

Doglioni, C., Panza, G., 2015. Polarized plate tectonics, in: Advances in Geophysics. Elsevier. volume 56, pp. 1–167.

Ficini, E., Cuffaro, M., Doglioni, C., 2020. Asymmetric dynamics at subduction zones derived from plate kinematic constraints. Gondwana Res. 78, 110–125.

Ficini, E., Dal Zilio, L., Doglioni, C., Gerya, T., 2017. Horizontal mantle flow controls subduction dynamics. Sci. Rep. 7, 1–7.

Goldreich, P., Soter, S., 1966. Q in the solar system. Icarus 5, 375–389.

Green, D.H., Hibberson, W.O., Kovács, I., Rosenthal, A., 2010. Water and its influence on the lithosphere–asthenosphere boundary. Nature 467, 448–451.

Gripp, A.E., Gordon, R.G., 2002. Young tracks of hotspots and current plate velocities. Geophys. J. Int. 150, 321–361.

Hirth, G., Kohlstedt, D.L., 1995. Experimental constraints on the dynamics of the partially molten upper mantle: 2. deformation in the dislocation creep regime. J. Geophys. Res.: Solid Earth 100, 15441–15449.

Höink, T., Jellinek, A.M., Lenardic, A., 2011. Viscous coupling at the lithosphere-asthenosphere boundary. Geochem. Geophys. Geosyst. 12(10), Q0AK02.

Hua, J., Fischer, K.M., Becker, T.W., Gazel, E., Hirth, G., 2023. Asthenospheric low-velocity zone consistent with globally prevalent partial melting. Nat. Geosci., 1–7

Ide, S., Tanaka, Y., 2014. Controls on plate motion by oscillating tidal stress: Evidence from deep tremors in western japan. Geophys. Res. Lett. 41, 3842–3850.

Jin, Z.M., Green, H.W., Zhou, Y., 1994. Melt topology in partially molten mantle peridotite during ductile deformation. Nature 372, 164–167.

Jordan, T.H., 1974. Some comments on tidal drag as a mechanism for driving plate motions. J. Geophys. Res. 79, 2141–2142.

Knopoff, L., Leeds, A., 1972. Lithospheric momenta and the deceleration of the earth. Nature 237, 93–95.

Kossobokov, V.G., Panza, G.F., 2020. A myth of preferred days of strong earthquakes? Seismol. Res. Lett. 91, 948–955.

Le Pichon, X., 1968. Sea-floor spreading and continental drift. J. Geophys. Res. 73, 3661–3697.

Lenci, F., Doglioni, C., 2007. On some geometric prism asymmetries. Thrust belts and foreland basins: from fold kinematics to hydrocarbon systems, Springer., 41–60

Mannix, P., Mestel, A., 2021. Bistability and hysteresis of axisymmetric thermal convection between differentially rotating spheres. J. Fluid Mech. 911, A12.

Mitrovica, J., Forte, A., 2004. A new inference of mantle viscosity based upon joint inversion of convection and glacial isostatic adjustment data. Earth Planet. Sci. Lett. 225, 177–189.

Munk, W., 1997. Once again: once again–tidal friction. Prog. Oceanogr. 40, 7–35.

Naif, S., Key, K., Constable, S., Evans, R., 2013. Melt-rich channel observed at the lithosphere–asthenosphere boundary. Nature 495, 356–359.

Nelson, T., Temple, P., 1972. Mainstream mantle convection: a geologic analysis of plate motion. AAPG Bulletin 56, 226–246.

Ogilvie, G.I., Lesur, G., 2012. On the interaction between tides and convection. Mon. Not. R. Astron. Soc. 422, 1975–1987.

Panza, G., Doglioni, C., Levshin, A., 2010. Asymmetric ocean basins. Geology 38, 59–62.

Pollitz, F.F., 2019. Lithosphere and shallow asthenosphere rheology from observations of post-earthquake relaxation. Phys. Earth Planet. Inter. 293, 106271.

Pollitz, F.F., Burgmann, R., Romanowicz, B., 1998. Viscosity of oceanic asthenosphere inferred from remote triggering of earthquakes. Science 280, 1245–1249.

Qiu, Q., Moore, J.D., Barbot, S., Feng, L., Hill, E.M., 2018. Transient rheology of the Sumatran mantle wedge revealed by a decade of great earthquakes. Nature Commun. 9, 995.

Ranalli, G., 2000. Westward drift of the lithosphere: not a result of rotational drag. Geophys. J. Int. 141, 535–537.

Ricard, Y., Doglioni, C., Sabadini, R., 1991. Differential rotation between lithosphere and mantle: a consequence of lateral mantle viscosity variations. J. Geophys. Res.: Solid Earth 96, 8407–8415.

Riguzzi, F., Panza, G., Varga, P., Doglioni, C., 2010. Can earth's rotation and tidal despinning drive plate tectonics? Tectonophysics 484, 60–73.

Scholz, C.H., Tan, Y.J., Albino, F., 2019. The mechanism of tidal triggering of earthquakes at mid-ocean ridges. Nature Commun. 10, 2526.

Scoppola, B., Boccaletti, D., Bevis, M., Carminati, E., Doglioni, C., 2006. The westward drift of the lithosphere: A rotational drag? Geol. Soc. Am. Bull. 118, 199–209.

Stevenson, D.J., 1994. Weakening under stress. Nature 372, 129–130.

Teunissen, P.J., Montenbruck, O., 2017. Springer handbook of global navigation satellite systems, volume 10. Springer.

Thybo, H., 2006. The heterogeneous upper mantle low velocity zone. Tectonophysics 416, 53–79.

Torsvik, T.H., Steinberger, B., Gurnis, M., Gaina, C., 2010. Plate tectonics and net lithosphere rotation over the past 150 my. Earth Planet. Sci. Lett. 291, 106–112.

Uyeda, S., Kanamori, H., 1979. Back-arc opening and the mode of subduction. J. Geophys. Res.: Solid Earth 84, 1049–1061.

Varga, P., Grafarend, E., 2019. Influence of tidal forces on the triggering of seismic events. Geodynamics and Earth Tides Observations from Global to Micro Scale, 55–63.

Verard, C., Hochard, C., Stampfli, G., 2012. Non-random distribution of euler poles: is plate tectonics subject to rotational effects? Terra Nova 24, 467–476.

Wang, Q., 2010. A review of water contents and ductile deformation mechanisms of olivine: implications for the lithosphere–asthenosphere boundary of continents. Lithos 120, 30–41.

Weismüller, J., Gmeiner, B., Ghelichkhan, S., Huber, M., John, L., Wohlmuth, B., Rüde, U., Bunge, H.P., 2015. Fast asthenosphere motion in high-resolution global mantle flow models. Geophys. Res. Lett. 42, 7429–7435.

Weiss, J.P., Steigenberger, P., Springer, T., 2017. Orbit and clock product generation, in: Springer handbook of global navigation satellite systems. Springer, pp. 983–1010.

Zaccagnino, D., Doglioni, C., 2022. Earth's gradients as the engine of plate tectonics and earthquakes. La Rivista del Nuovo Cimento, 1–81.

Zaccagnino, D., Telesca, L., Doglioni, C., 2022. Correlation between seismic activity and tidal stress perturbations highlights growing instability within the brittle crust. Scientific Reports 12, 1–14.

Zaccagnino, D., Telesca, L., Doglioni, C., 2022. Variable seismic responsiveness to stress perturbations along the shallow section of subduction zones: the role of different slip modes and implications for the stability of fault segments. Frontiers. Earth Sci. 2192.

Zaccagnino, D., Vespe, F., Doglioni, C., 2020. Tidal modulation of plate motions. Earth-Sci. Rev. 205, 103179.